MBoC | ARTICLE

High extracellular glucose promotes cell motility by modulating cell deformability and contractility via the cAMP-RhoA-ROCK axis in human breast cancer cells

Mijung Oh[a], Skylar Batty[b,c,†], Nayan Banerjee[a,d], and Tae-Hyung Kim[a,e,*]

[a]Department of Pathology, School of Medicine and [b]Undergraduate Pipeline Network Summer Research Program, University of New Mexico Health Sciences Center, Albuquerque, NM 87131; [c]Department of Molecular and Cellular Biology, University of Arizona, Tucson, AZ 85721; [d]School of Chemical Sciences, Indian Association for the Cultivation of Science, Jadavpur, Kolkata 700032, West Bengal, India; [e]University of New Mexico Comprehensive Cancer Center, Albuquerque, NM 87131

ABSTRACT **The mechanical properties, or mechanotypes, of cells are largely determined by their deformability and contractility. The ability of cancer cells to deform and generate contractile force is critical in multiple steps of metastasis. Identifying soluble cues that regulate cancer cell mechanotypes and understanding the underlying molecular mechanisms regulating these cellular mechanotypes could provide novel therapeutic targets to prevent metastasis. Although a strong correlation between high glucose level and cancer metastasis has been demonstrated, the causality has not been elucidated, and the underlying molecular mechanisms remain largely unknown. In this study, using novel high-throughput mechanotyping assays, we show that human breast cancer cells become less deformable and more contractile with increased extracellular glucose levels (>5 mM). These altered cell mechanotypes are due to increased F-actin rearrangement and nonmuscle myosin II (NMII) activity. We identify the cAMP-RhoA-ROCK-NMII axis as playing a major role in regulating cell mechanotypes at high extracellular glucose levels, whereas calcium and myosin light-chain kinase (MLCK) are not required. The altered mechanotypes are also associated with increased cell migration and invasion. Our study identifies key components in breast cancer cells that convert high extracellular glucose levels into changes in cellular mechanotype and behavior relevant in cancer metastasis.**

Monitoring Editor
Valerie Marie Weaver
University of California, San Francisco

Received: Dec 19, 2022
Revised: Apr 18, 2023
Accepted: May 8, 2023

INTRODUCTION

The triple-negative breast cancer (TNBC) subtype is characterized by the lack of expression of estrogen receptor (ER) and progesterone receptor (PR), as well as the absence of HER2 overexpression. This limits the development of targeted therapy for this subtype, as these receptors are prime targets for the treatment of other, more prominent, breast cancer subtypes (Lyons, 2019). TNBC is the most aggressive subtype, characterized by the highest rate of distant metastasis and the shortest overall survival (Carey *et al.*, 2007;

This article was published online ahead of print in MBoC in Press (http://www.molbiolcell.org/cgi/doi/10.1091/mbc.E22-12-0560) on May 17, 2023.

†Present address: Biomedical Sciences Graduate Program, University of California San Diego, La Jolla, CA 92093.

Author contributions: M.O. and T.-H.K. designed the experiments; M.O., S.B., and T.-H.K. performed experiments; M.O., S.B., N.B., and T.-H.K. analyzed and interpreted the data; M.O., S.B., N.B., and T.-H.K. wrote the manuscript.

Conflicts of interest: The authors declare no conflicts of interest.

*Address correspondence to: Tae-Hyung Kim (takim@salud.unm.edu).

Abbreviations used: AC, adenylyl cyclase; βAR, β-adrenergic receptor; cAMP, cyclic adenosine monophosphate; CNGC, cyclic nucleotide gated ion channel; 2DG, 2-deoxy-D-glucose; DMEM/F12, Dulbecco's modified eagle medium F-12; ECAR, extracellular acidification rate; Epac, exchange protein directly activated by cAMP; ER, estrogen receptor; F-actin, filamentous actin; FBS, fetal bovine serum; FLECS, fluorescent elastomeric contractible surfaces; FRET, Förster resonance energy transfer; GLUT, glucose transporter; MLCK, myosin light-chain kinase; NMII, non-muscle myosin II; OCR, oxygen consumption rate; PAK1, p21-actiavted kinase; PDE, phosphodiesterase; PMF, parallel microfiltration; pMLCK, phosphorylated MLCK; POPDC, Popeye domain containing; PR, progesterone receptor; PVDF, polyvinylidene difluoride; ROCK, Rho-associated coiled coil-forming kinase; TNBC, triple-negative breast cancer.

Núñez Abad *et al.*, 2021). Development of novel therapeutic strategies to suppress metastasis is urgently needed to improve the current treatment outcomes in TNBC patients.

Epidemiologic evidence shows the association between obesity and certain cancers including breast cancer (Giovannucci *et al.*, 2010; Sarfati *et al.*, 2016). In 2021, the World Gastroenterology Organization declared obesity as a pandemic (The Lancet Gastroenterology and Hepatology, 2021) and there has been a rising global interest in defining the biological mechanisms shared between cancer and obesity. A recent meta-analysis study has shown the strong negative prognostic role of obesity in TNBC (Harborg *et al.*, 2021), and the association between TNBC and obesity is reviewed elsewhere (Sun *et al.*, 2017). Due to the distinctive presence of adipose-rich connective tissue known as the mammary fat pad within breast tissue (Choi *et al.*, 2018), adipocyte-secreted factors such as growth factors and adipokines have been heavily investigated and now characterized as molecular mediators connecting obesity and breast cancer progression (Wu *et al.*, 2019; Bhardwaj and Brown, 2021; Zhao *et al.*, 2020; Zhang *et al.*, 2022). However, in addition to adiposopathy, obesity is also accompanied by elevated blood glucose levels, known as hyperglycemia (Martyn *et al.*, 2008). Glucose is an essential fuel for nearly all cell types, and blood glucose levels are tightly regulated to ensure metabolic homeostasis (Nordlie *et al.*, 1999). Glucose also plays a critical role in cancer cell metabolism, as described by the Warburg effect (Liberti and Locasale, 2016), where cancer cells uptake glucose as their main energy source to support increased glycolysis. Indeed, high glucose levels promote aggressiveness of breast cancer cells, which includes increased cell proliferation (Okumura *et al.*, 2002; Sun *et al.*, 2019), drug resistance (Qiu *et al.*, 2021), and motility (Sun *et al.*, 2019; Takatani-Nakase *et al.*, 2014). Because TNBC is highly metastatic and glucose regulates breast cancer cell behavior, there is an urgent need to understand the molecular mechanisms by which high glucose level enhances TNBC cell invasion, and ultimately metastasis, in order to devise novel therapeutic options for this hard-to-target breast cancer subtype.

Metastasis is a multistep process that includes invasion of the basement membrane, intravasation, survival in circulation, extravasation, and colonization of a secondary tumor site (Hapach *et al.*, 2019; Welch and Hurst, 2019). Recent studies have demonstrated that cell mechanotypes play a critical role in multiple stages of metastasis (Kumar and Weaver, 2009; Follain *et al.*, 2020). Two key components involved in metastasis are cell deformability and contractility, which are defined as the ability of cancer cells to deform and to generate contractile forces, respectively. Cancer cells that are more deformable or "softer" are more metastatic (Ochalek *et al.*, 1988; Liu *et al.*, 2020), and cancer cells with increased traction forces tend to be more invasive (Okeyo *et al.*, 2009; Kraning-Rush *et al.*, 2012). In contrast, we discovered that activation of β-adrenergic receptor (βAR) signaling in various cancer cells resulted in increased cell stiffness and contractility, which are positively correlated with increased migration and invasion (Kim *et al.*, 2016). Others have also demonstrated that stiffer cells can be more invasive in particular cancer types (Ekpenyong *et al.*, 2012; Monzo *et al.*, 2021), suggesting that the relationship between cancer cell mechanotypes and invasion may be context-dependent. Because cell mechanotype plays a critical role in controlling cancer cell invasion, we aim to investigate the effects of high glucose concentration on cancer cell mechanotypes as well as the underlying molecular mediators.

In this study, we show that high glucose decreases deformability and increases contractility of breast cancer cells in vitro via increased filamentous actin (F-actin) levels and nonmuscle myosin II (NMII) activity. These altered mechanotypes are associated with increased cell migration and invasion, which is consistent with our βAR study (Kim *et al.*, 2016). On a molecular level, we have discovered that the activation of the RhoA-ROCK-NMII axis is needed to translate high extracellular glucose levels into cell mechanotype changes, whereas calcium ion–dependent myosin light-chain kinase (MLCK) and Rac1-dependent p21-activated kinase 1 (PAK1) are not involved. We also report that increased intracellular cyclic adenosine monophosphate (cAMP) levels activate the RhoA-NMII axis, implying that the cAMP pathway is involved in the regulation of cell mechanotypes. These results provide a basis for future studies to identify therapeutic targets to suppress hyperglycemia-induced TNBC metastasis in preclinical models.

RESULTS

Breast cancer cells become less deformable and more contractile with an increase in extracellular glucose levels

High glucose levels promote migration and invasion of breast cancer cells in vitro (Takatani-Nakase *et al.*, 2014; Sun *et al.*, 2019). However, the underlying molecular mechanisms are not fully understood. Because cellular mechanotypes dictate cell motility (Blanchoin *et al.*, 2014), we investigated whether high extracellular glucose levels alter breast cancer cell mechanotypes, including cell deformability and contractility. During metastasis, cancer cells experience elevation of glucose concentrations, as glucose diffuses from blood circulation (~5 mM) to peripheral tissues (~1–2 mM; Hirayama *et al.*, 2009). Indeed, breast cancer cells exhibit heterogeneity in their intracellular glucose levels in vivo: cancer cells in the tumor boundary exhibit high intracellular glucose levels, whereas cancer cells in the tumor core exhibit low intracellular glucose levels (Kondo *et al.*, 2021). To mimic this physiological condition in vitro, we depleted extracellular glucose by cultivating human breast cancer cell lines in 5.5-mM glucose media for 48 h. During this glucose starvation, cells proliferate and consume glucose, resulting in depletion of glucose from culture media (Supplemental Figure S1A). When cells experience less than 1 mM of glucose in culture media, we change the culture media to treat cells with different glucose concentrations. Therefore, in our experimental system, breast cancer cells experience increases in glucose concentrations, which mimic the early metastasis steps in vivo.

Nonmalignant mammary epithelial cells (MCF10A), noninvasive luminal-type breast cancer cells (MCF7), and invasive basal-type TNBC cells (MDA-MB-231), as well as their highly metastatic variant, MDA-MB-231/HM cells (Chang *et al.*, 2008) were treated with different concentrations of D-glucose, reflecting peripheral tissue (1 mM), blood (5 mM), hyperglycemic (11 mM), and standard culture conditions (25 mM). Because glucose deprivation induces cancer cell death (Palorini *et al.*, 2013; Chen *et al.*, 2020), we measured cell viability and cell cycle after 24 h treatment of different glucose levels in MCF7, MDA-MB-231, and MDA-MB-231/HM cells. Cell viability was not changed with low glucose levels (Supplemental Figure S1B), and we observed cell cycle arrest only in MDA-MB-231/HM cells treated with 1 mM glucose for 24 h (Supplemental Figure S1C). All three breast cancer cell lines tested showed a decrease in whole cell deformability with an increase in glucose concentrations measured by parallel microfiltration (PMF) assay (Figure 1A) in a concentration-dependent manner, whereas the deformability of MCF10A was not changed (Figure 1C). No changes in cell size with high glucose levels were observed, suggesting that the increased retention in the PMF assay is due to reduced whole cell deformability (Supplemental Figure S2A). Because glucose is metabolized by glycolysis following its uptake, we inhibited glycolysis using 2-deoxy-D-glucose (2DG), which inhibits the key glycolysis enzymes hexokinase and glucose-6-phosphate isomerase (Wick *et al.*, 1957). Inhibition of glycolysis diminished the cell-stiffening effect of high glucose in TNBC cells (Figure 1C). We

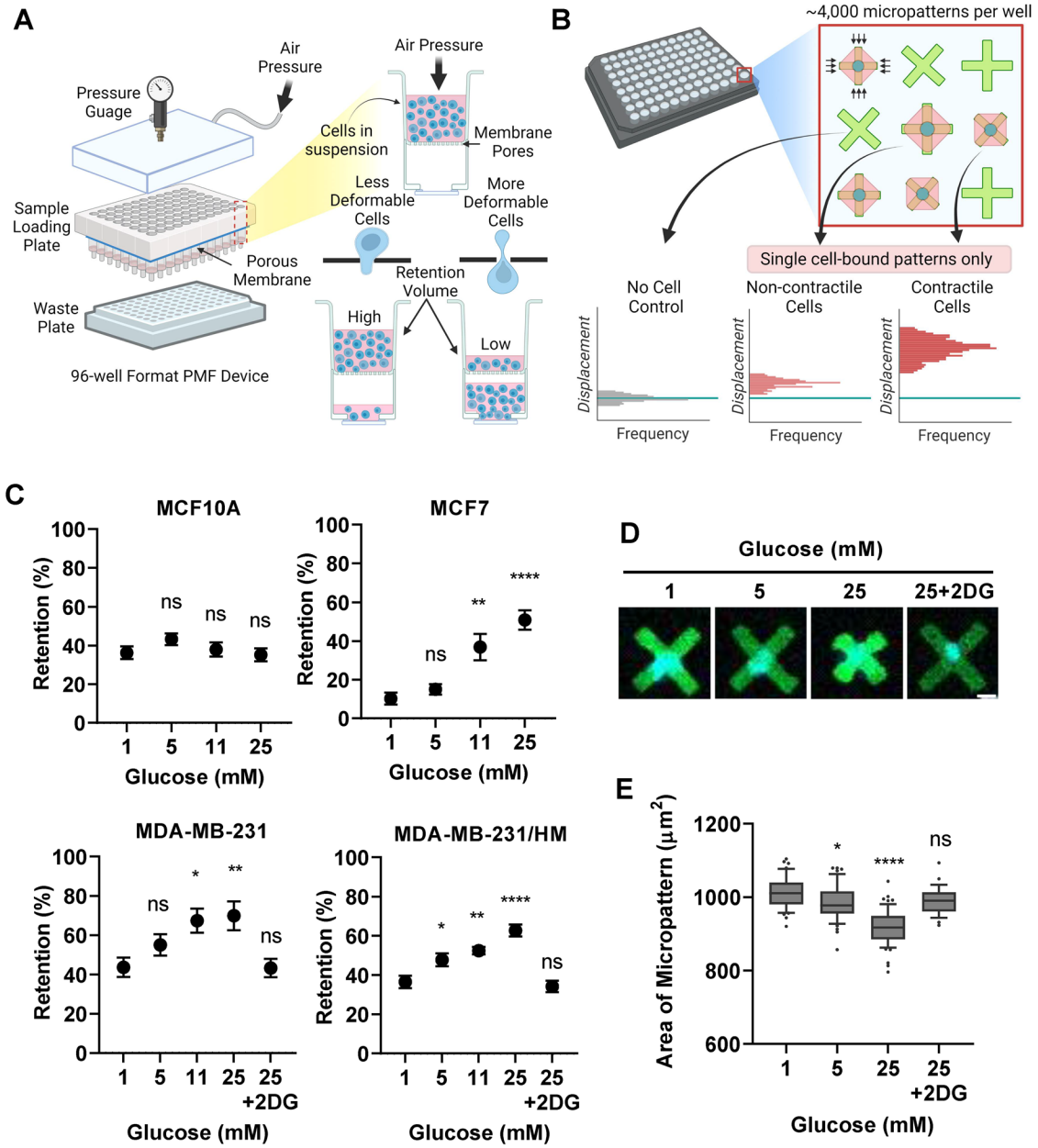

FIGURE 1: Altered mechanotypes of breast cancer cells at different glucose levels. (A) Schematic illustration of whole-cell deformability measurement using PMF. Less deformable, or stiffer, cells occlude membrane pores, resulting in a higher retention rate. (B) Schematic illustration of whole-cell contractility measurement using FLECS. (C) Using PMF, the deformability of cells treated with high glucose for 3 h was measured. Less deformable, or stiffer, cells occlude the membrane pores, resulting in a higher retention rate. Error bars represent mean ± SEM. (D) Using FLECS, the contractility of MDA-MB-231 cells treated with high glucose for 3 h was measured. More contractile cells induce higher displacement of the fluorescence-labeled micropatterns, resulting in smaller pattern sizes. Scale bar, 10 μm. (E) Quantitation of single-cell adhered micropattern sizes ($n = 58$). The center line denotes the median value. The whiskers show the 10–90th percentiles. Statistical significance was determined by a one-way ANOVA test (ns, not significant; *, $p < 0.05$; **, $p < 0.01$, ****, $p < 0.0001$). A and B were created with BioRender.com.

focused on investigating the invasive MDA-MB-231 cells in the following experiments, as cell mechanotypes are important in these metastatic cell types specifically. Next, we measured another important cell mechanotype, whole cell contractility, using fluorescent elastomeric contractible surfaces (FLECS) assay (Figure 1B). Compared with 1 mM glucose, we observed significantly increased whole cell contractility from MDA-MB-231 cells treated with 5 mM and 25 mM of glucose (Figure 1, D and E). Inhibition of glycolysis with 2DG resulted in diminished effects of high glucose on whole cell contractility (Figure 1, D and E), suggesting that glycolysis is required for these mechanotype changes. Taken together, these data suggest that breast cancer cells change their mechanotypes–decreased deformability and increased contractility–with elevated extracellular glucose levels.

High glucose increases nonmuscle myosin II activity and F-actin levels

Actin and myosin filaments assemble structures forming actomyosin filaments, which play a pivotal role in regulating cellular force

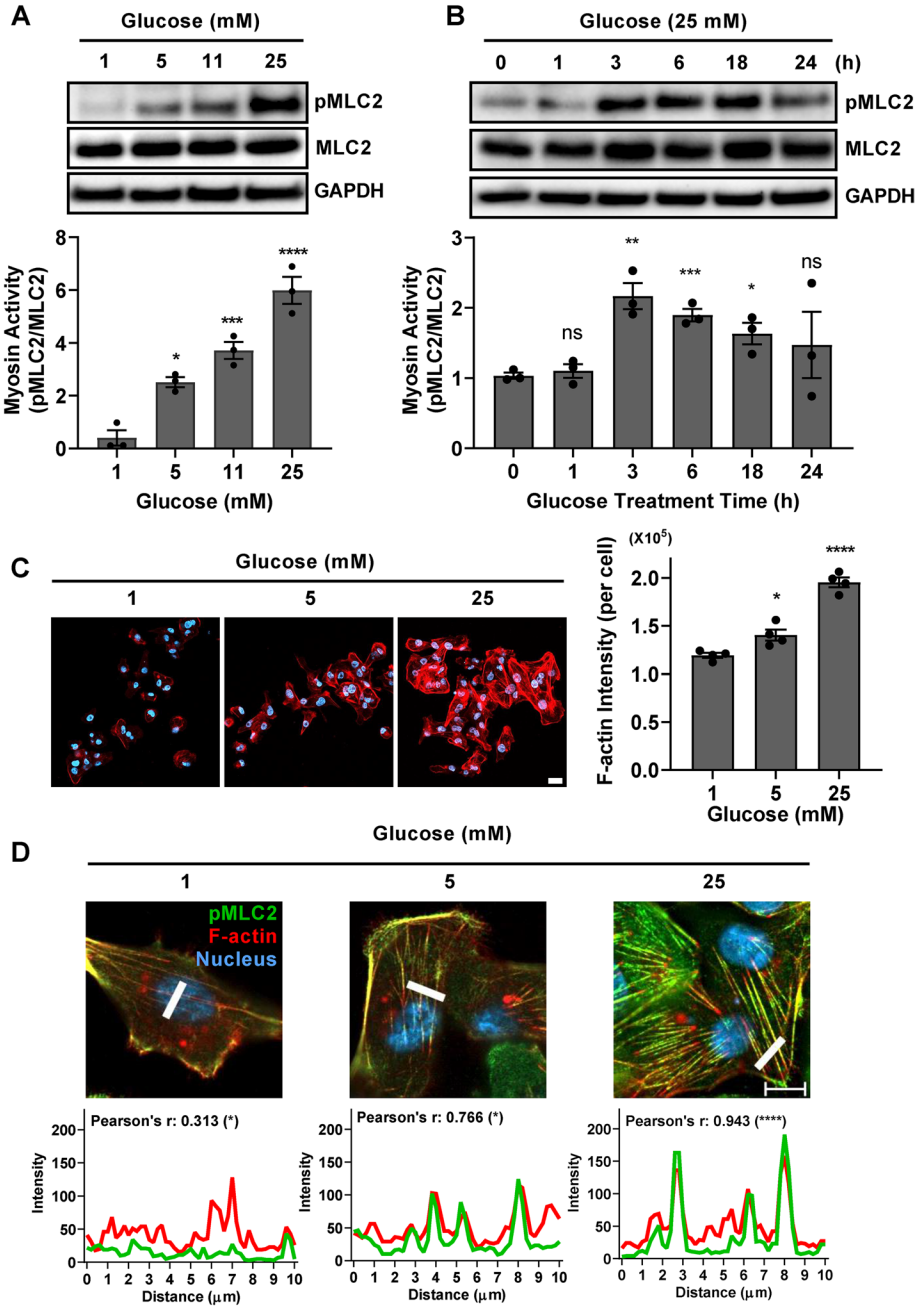

FIGURE 2: High glucose levels increase myosin activity and F-actin levels. (A) Nonmuscle myosin activity after glucose treatment for 3 h was measured by probing the phosphorylation level of myosin light chain 2 (MLC2). Quantified band intensity with statistical test is shown below ($n = 3$). (B) pMLC2 level was measured at the indicated time points after 25 mM glucose treatment. Quantified band intensity with statistical test is shown below ($n = 3$). Statistical significance was determined by unpaired *t* test. (C) Representative confocal microscopy images of MDA-MB-231 cells treated with different glucose levels for 3 h. Scale bar, 20 μm. F-actin intensity normalized to cell number is shown on the right panel ($n = 4$). (D) To compare the subcellular localization of pMLC2 (green) and F-actin (red), fluorescence intensity of each target in a marked region (white line) was analyzed using line intensity profiles (below each image). Pearson's correlation coefficient representing colocalization efficiency is denoted. Scale bar, 10 μm. All error bars represent mean ± SEM. Unless otherwise stated, all statistical significance was determined by one-way ANOVA test (ns, not significant; *, $p < 0.05$; **, $p < 0.01$; ***, $p < 0.001$; ****, $p < 0.0001$).

generation and cell migration (Murrell *et al.*, 2015). Previously, we have demonstrated that increased F-actin levels and myosin activity confer increased breast cancer cell stiffness and contractility upon activation of β-adrenergic signaling (Kim *et al.*, 2019, 2016). When MDA-MB-231 cells were treated with increasing concentrations of glucose, phosphorylation of nonmuscle myosin regulatory light chain 2 (MLC2), which regulates the activity of NMII, was increased in a concentration-dependent manner (Figure 2A). Similarly, phosphorylation of MLC2 was increased with high glucose levels in a concentration-dependent manner in MDA-MB-231/HM and MCF7 cells (Supplemental Figure S2, D and E). Interestingly, while >5 mM glucose increased pMLC2 levels compared with 1 mM glucose in MCF10A cells (Supplemental Figure S2F), concentration dependency was not observed in this nontumorigenic cell type, suggesting less dependence on glucose. Glucose-induced myosin activation in MDA-MB-231 cells was greatest at 3 h and decreased in 24 h (Figure 2B). In contrast to MDA-MB-231 cells, no significant change in whole cell contractility was observed from MCF10A cells treated with high glucose (Supplemental Figure S2C) despite the significant increase in pMLC2 level (Supplemental Figure S2F). Similarly, the whole cell contractility of MDA-MB-231/HM cells was not altered by high-glucose treatment (Supplemental Figure S2B). Because the basal expression level of MLC2 is significantly low in MDA-MB-231/HM and MCF10A cells compared with that in MDA-MB-231 cells (Supplemental Figure S4, G and, H), we speculate that MDA-MB-231/HM and MCF10A cells were incapable of generating enough force to contract the substrate of FLECS device despite the significant increase in pMLC2 activity (Supplemental Figure S2, D and F).

Next, we measured F-actin levels in breast cancer cell lines as well as in MCF10A cells treated with different glucose levels. Similarly to the activation of myosin, cellular F-actin levels were increased in a glucose concentration–dependent manner after glucose treatment for 3 h in MDA-MB-231 cells (Figure 2C) and such an increase in F-actin levels was still observed at a later time point (24 h) in both MDA-MB-231 and MDA-MB-231/HM cells (Supplemental Figure S3, A and B). For an unbiased measurement of cellular F-actin levels, F-actin was stained with fluorescent dye–conjugated phalloidin, followed by quantitative fluorescence measurement using high-content image analysis. The F-actin levels per cell were significantly increased with increased glucose concentrations (Supplemental Figure S3, A and B) without changing gene expression levels (Supplemental Figure S3C), suggesting that increased F-actin levels are regulated at the posttranscriptional level. Further

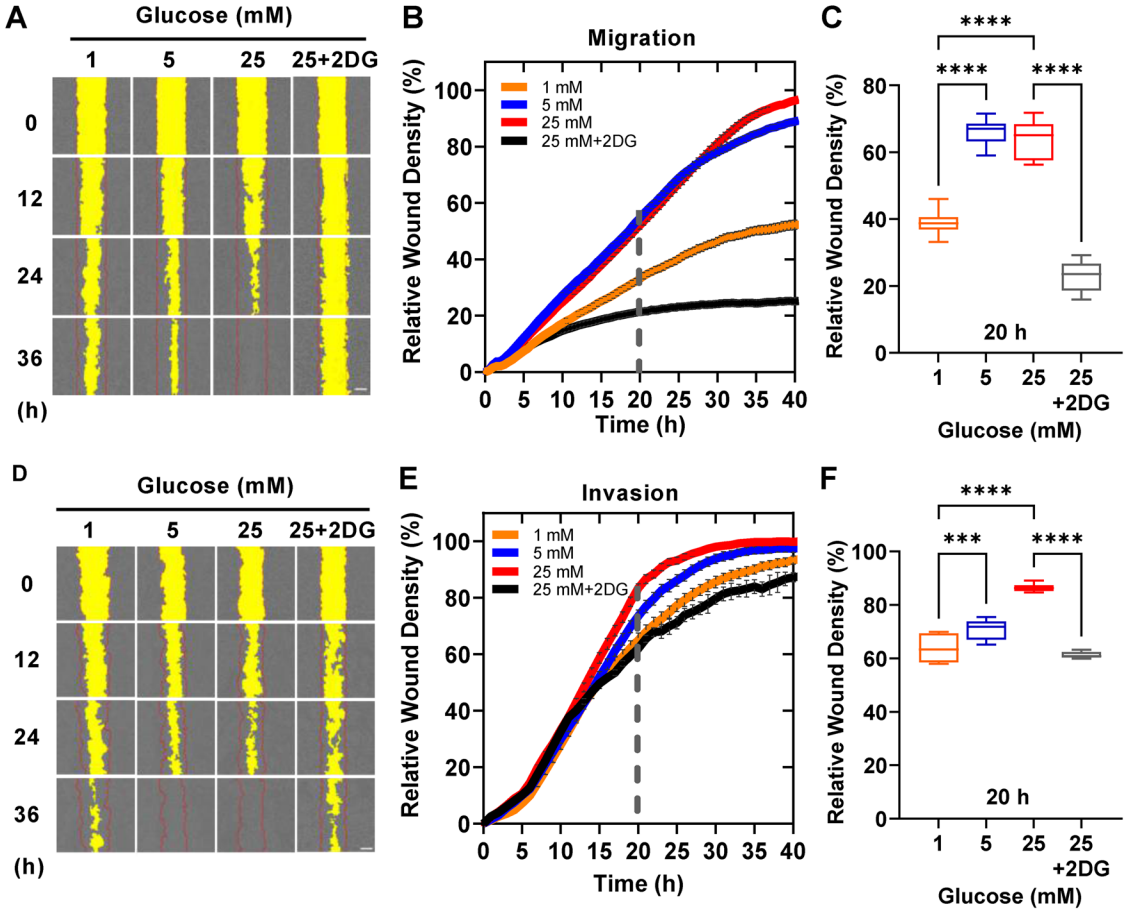

FIGURE 3: High glucose promotes cell migration and invasion. (A) Representative images from scratch wound migration assay of MDA-MB-231 cells (red line: initial scratch wound area; yellow: wound area; gray: area that is confluent with cells). Scale bar: 300 μm. (B) Relative wound density as a function of time. The dashed gray line indicates the time point (20 h) that is shown in (C) for a statistical test ($n = 8$). (D) Representative images from scratch wound invasion assay of MDA-MB-231 cells. (E) Relative wound density as a function of time. The dashed gray line indicates the time point (20 h) that is shown in (F) for statistical test ($n = 8$). In the box and whiskers plot, the center line denotes the median value and the whiskers show the 10th–90th percentiles. Statistical significance was determined by one-way ANOVA test (***, $p < 0.001$; ****, $p < 0.0001$).

investigation using images obtained from confocal microscopy revealed that F-actin levels increase in high glucose–treated cells in both cytoplasmic and cortical regions (Supplemental Figure S3B). High glucose–induced F-actin polymerization was observed only in breast cancer cell lines (Supplemental Figure S3, E and F), and no changes were observed in MCF10A cells (Supplemental Figure S3G). Interestingly, the basal F-actin level was higher in MDA-MB-231/HM cells than in MDA-MB-231 cells (Supplemental Figure S4F) without differences in gene expression level (Supplemental Figure S4E), and the magnitude of F-actin increase between low and high glucose treatment was also higher in MDA-MB-231/HM cells than in its parental cell line of MDA-MB-231 cells (Supplemental Figure S3, A and B). To investigate whether these altered cytoskeletal rearrangements and myosin activity contribute to actomyosin formation, we performed image analysis from F-actin and pMLC2 costained MDA-MB-231 cells. This revealed colocalization of active myosin with F-actin, suggesting the formation of actomyosin fibers (Figure 2D). Taken together, these results show that high extracellular glucose levels enhance F-actin polymerization and phosphorylation of myosin light chain to increase contractility and stiffness in TNBC cells.

High glucose promotes migration and invasion of metastatic breast cancer cells

Because cellular mechanotype is strongly associated with cancer cell motility (Yu *et al.*, 2020, 2022), we next measured the effect of high glucose levels on promoting TNBC cell migration and invasion. Boyden chambers without extracellular matrices were used for cell migration assays. MDA-MB-231 cells treated with high glucose levels showed increased cell migration (Supplemental Figure S3D). To measure the effect of high glucose on collective cell migration, we used a scratch wound healing assay as previously described (Kim *et al.*, 2016). Consistent with previous work by others (Sun *et al.*, 2019; Takatani-Nakase *et al.*, 2014) and our transwell migration data (Supplemental Figure S3D), we observed that high glucose promotes collective cell migration in a concentration-dependent manner in both MDA-MB-231 (Figure 3, A–C) and MDA-MB-231/HM cells (Supplemental Figure S4A). Glucose-induced cell migration was diminished when glycolysis was inhibited by 2DG. Additionally, high glucose promoted cell invasion in both MDA-MB-231 and MDA-MB-231/HM cells (Figure 3, D–F; Supplemental Figure S4B). Interestingly, MDA-MB-231/HM cells showed faster migration activity than MDA-MB-231 cells (Supplemental Figure S4C), yet

MDA-MB-231/HM invasion was slower than MDA-MB-231 invasion (Supplemental Figure S4D).

Glycolysis is required for glucose-induced mechanotype changes

Extracellular glucose molecules are catabolized via glycolysis immediately after uptake by cells (Shin and Koo, 2021). Because high extracellular glucose level impacts breast cancer cell mechanotype and motility, we asked if glycolysis is required for mechanotype changes. First, we confirmed the expression levels of glucose transporters (GLUTs) in our cell lines. GLUTs are up-regulated in breast cancer cells, and the overexpression of GLUT-1, -3, and -12 has been associated not only with the early tumorigenesis but also with the invasiveness and poor prognosis of breast cancer (Krzeslak *et al.*, 2012; Macheda *et al.*, 2005; Medina and Owen, 2002; Pinheiro *et al.*, 2011; Szablewski, 2013). Because breast cancer cells rely most heavily on glycolysis, which produces fewer ATP molecules per glucose molecule than oxidative phosphorylation, up-regulation of GLUT is essential for these cells to meet the increased demand for glucose uptake. Indeed, GLUT1 plays a pivotal role in glucose uptake in breast cancer cells and is the main glucose transporter in MCF7 and MDA-MB-231 cell lines (Grover-McKay *et al.*, 1998; Wuest *et al.*, 2018). Consistent with previous studies, our gene expression analysis confirmed that MCF7 and MDA-MB-231 cells express GLUT-1, -3, -4, and -12 (Supplemental Figure S5A; Laudański *et al.*, 2003; Garrido *et al.*, 2015; Matsui *et al.*, 2017). GLUT1 and GLUT3 have high affinity for glucose molecules, with a K_m value of 1–2 mM, which allows effective facilitative glucose transport down its concentration gradient (Brown, 2000; Gorovits and Charron, 2003). We observed increased glycolysis rates when extracellular glucose levels were increased in MDA-MB-231 (Figure 4A), MDA-MB-231/HM (Supplemental Figure S5B), and MCF7 (Supplemental Figure S5C) cells, as measured by extracellular acidification. In contrast, glycolysis rate was not altered with increased extracellular glucose levels in MCF10A cells (Supplemental Figure S5D), suggesting that cancer cells rely more heavily on glucose availability than nonmalignant cells. The changes in cellular glycolysis rates induced by different extracellular glucose levels were sustained for 10 h (Figure 4A). A recent study has shown that increased glycolysis serves as a main energy source in breast cancer cell invasion, while oxidative phosphorylation provides basic cellular energy for sustenance of breast cancer cells (Fujita *et al.*, 2020). Consistent with this study, we observed the highest rate of glucose-dependent glycolysis of all cell types tested (Supplemental Figure S5, B–D) in the highly invasive cancer cell line MDA-MB-231 (Figure 4A). We also observed decreased oxygen consumption in high extracellular glucose conditions in all cell types tested (Figure 4B; Supplemental Figure S5, E–G), suggesting that increased glycolysis is the main driving force to promote cell migration in breast cancer cells.

Nonmuscle MLC2 is phosphorylated by multiple kinases, including MLCK (Newell-Litwa *et al.*, 2015). Therefore, we asked if high extracellular glucose levels activate MLC2 through the MLCK pathway. MLCK is a Ca^{2+}/calmodulin-dependent kinase and phosphorylation of MLCK at serine 1760 decreases its binding affinity to Ca^{2+}/calmodulin, resulting in decreased kinase activity (Raina *et al.*, 2009). When we measured the intracellular Ca^{2+} levels and phosphorylated MLCK (pMLCK) levels across several glucose concentrations, we observed no changes in pMLCK levels and intracellular calcium ion levels in MDA-MB-231 (Figure 4, C and D) and MDA-MB-231/HM (Supplemental Figure S6, A and B) cells across all glucose concentrations tested, while pMLC2 levels increased with increasing extracellular glucose concentration. Inhibition of glycolysis with 2DG had no effect on MLCK activity and intracellular Ca^{2+} levels in both MDA-MB-231 (Figure 4, C and D) and MDA-MB-231/HM (Supplemental Figure S6, A and B) cells. This suggests that MLCK is not involved in glucose-induced MLC2 activation. In addition, the glucose-induced increase in pMLC2 level was diminished when glycolysis was inhibited by 2DG in both MDA-MB-231 (Figure 4E) and MDA-MB-231/HM (Supplemental Figure S6C) cells, which is consistent with our whole-cell contractility result (Figure 1, D and E). Taken together, these data suggest that glycolysis is required for high glucose-induced mechanotype alterations in TNBC cells, independent of MLCK activity.

High glucose alters the mechanotype of breast cancer cells via the RhoA-ROCK-NMII axis

Previous studies have reported that changes in extracellular glucose levels result in global changes in gene expression levels in various human cell types, including breast cancer cells (Raina *et al.*, 2009; Hall *et al.*, 2018; Zhang *et al.*, 2021; Aoun *et al.*, 2022). However, we observed the altered cell mechanotypes in breast cancer cells as early as 3 h after high-glucose treatment. Therefore, we hypothesized that the mechanotype changes are posttranscriptionally regulated. To identify the molecular mediators, we conducted phosphoproteomic analysis. MDA-MB-231 cells were treated with 1 or 25 mM of glucose for 3 h, followed by snap-freezing. We identified 659 differentially phosphorylated proteins with statistical significance (p value < 0.05) out of the total 7868 measured phosphoproteins in 25 mM–glucose treated cells. Consistent with our previous works, which have shown that βAR signaling regulates breast cancer cell mechanotype via RhoA GTPase and the Rho-associated coiled coil-forming kinase (ROCK) axis (Kim *et al.*, 2016, 2019), pathway enrichment analysis using the BioJupies system (Torre *et al.*, 2018) showed that 25 and 29 differentially phosphorylated proteins by high glucose are involved in regulation of Rho GTPase and cytoskeleton organization, respectively (Supplemental Figure S6D). The full lists of these proteins are shown in Supplemental Tables 2 and 3.

We next measured the activity of RhoA GTPase in cells treated with high glucose. GTP-RhoA pull-down assay showed that 25 mM–glucose treatment for 3 h resulted in about a 2.0-fold increase in RhoA activity in both MDA-MB-231 and MDA-MB-213/HM cells compared with 1 mM glucose treatment (Figure 5A; Supplemental Figure S6E). When RhoA is activated pharmacologically by CN03 Rho Activator II, which constitutively activates Rho GTPase and does not affect the activity of Rac or Cdc42 (Flatau *et al.*, 1997; Schmidt *et al.*, 1997), increased myosin activity is observed (Figure 5B). Because RhoA activates the kinase activity of its downstream effector, ROCK, which in turn activates MLC2, we measured the ROCK activity and phosphorylation of MLC2 after high–extracellular glucose treatment. Consistent with our myosin-activation-with-high-glucose data (Figure 2A), we observed increased ROCK activity and phosphorylation of MLC2 with high glucose in a concentration-dependent manner in both MDA-MB-231 (Figure 5, C and D) and MDA-MB-213/HM cells (Supplemental Figure S6, F and G). The high glucose–induced activation of ROCK and MLC2 was diminished when glycolysis was inhibited by 2DG, or when ROCK activity was inhibited by Y27632 in both cell lines (Figure 5, C and D; Supplemental Figure S6, F and G). Cell deformability assay using PMF after inhibition of ROCK with Y27632 and inhibition of MLCK with ML7 showed that ROCK inhibition diminishes the high glucose–induced cell stiffening effect, while MLCK inhibition had no effect on cell deformability (Figure 5E). Furthermore, the activation of Rho GTPase with CN03 induced a cell-stiffening effect that was more significant

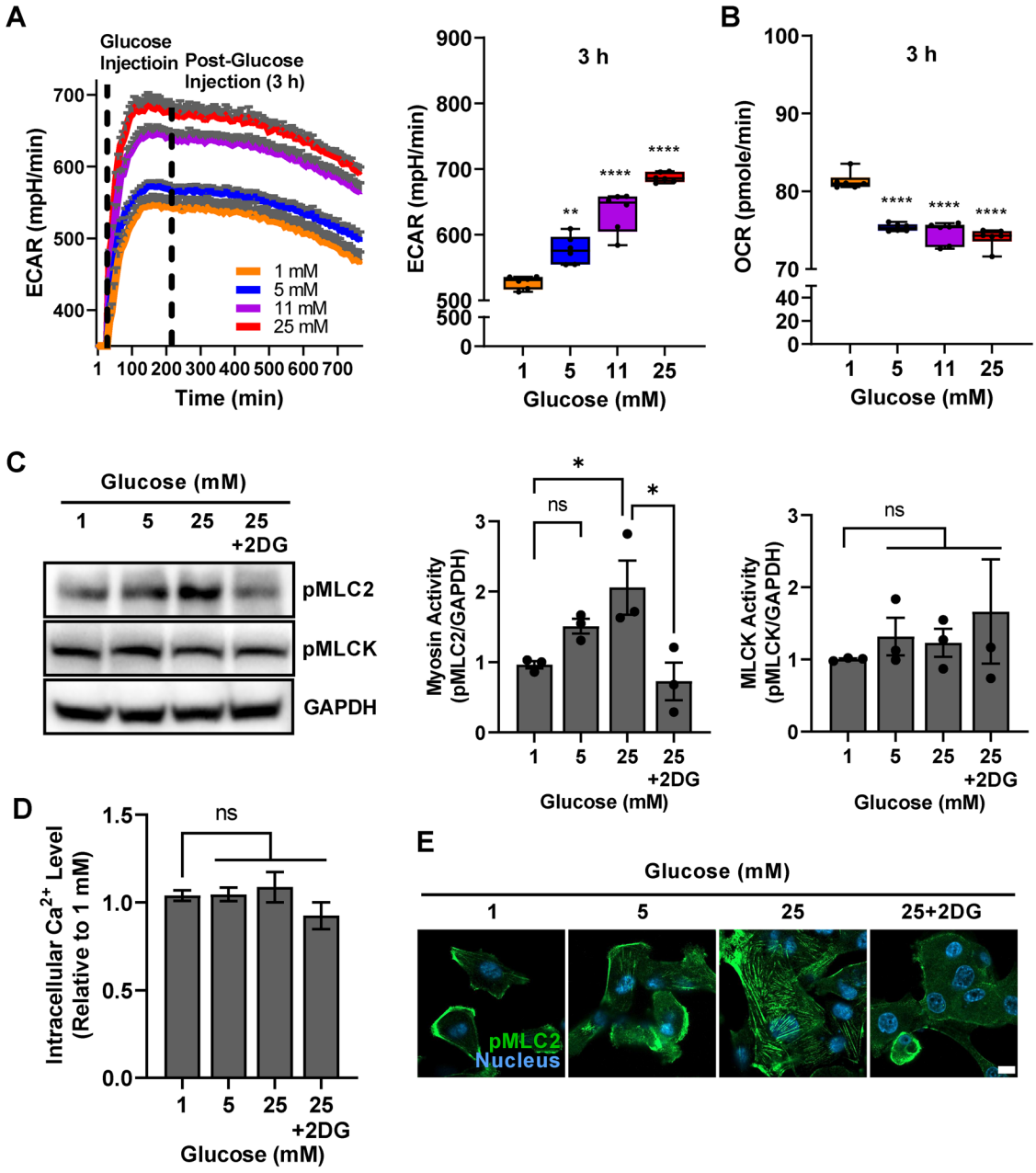

FIGURE 4: Glycolysis is required for myosin activation in breast cancer cells. (A) Glycolysis rate measured by extracellular acidification rate increases with higher extracellular glucose levels in MDA-MB-231. Extracellular acidification rate 3 h post–glucose injection with different glucose levels is shown in the right panel ($n = 6$). (B) Oxygen consumption rate 3 h post–glucose injection with different glucose levels ($n = 6$). Minimum, maximum, and median values are shown in box and whisker plots. (C) pMLC2 and pMLCK levels were measured by immunoblotting after treatment with different glucose concentrations and glycolysis inhibitor (2DG) for 3 h. Quantitation of Western blotting band intensity is shown on the right ($n = 3$). (D) Intracellular calcium ion levels were measured after treatment with different glucose concentrations and 2DG. (E) Representative images of pMLC2 staining in MDA-MB-231 cells treated with glucose for 3 h. Scale bar, 10 μm. All error bars represent mean ± SEM. Statistical significance was determined by one-way ANOVA test (ns, not significant; *, $p < 0.05$; **, $p < 0.01$; ***, $p < 0.001$).

under the low-glucose (1 mM) condition (Figure 5F) than under the high-glucose (25 mM) condition (Figure 5, E and F). The increased collective cell invasion by high glucose levels was blunted by ROCK inhibition with Y27632 in both MDA-MB-231 (Figure 5, G and H) and MDA-MB-231/HM (Supplemental Figure S6H) cells. Taken together, these data suggest that high extracellular glucose alters breast cancer cell mechanotypes through the RhoA-ROCK-MLC2 axis.

Modulation of cAMP level results in cell mechanotype changes

High extracellular glucose increases intracellular cAMP levels in mouse β-cells and CHO cells (Nakagawa *et al.*, 2015; Lin *et al.*, 2017), and cAMP plays an important role in many physiological and pathological processes including cell migration (Zhang *et al.*, 2020). To gain more insight into how high extracellular glucose regulates

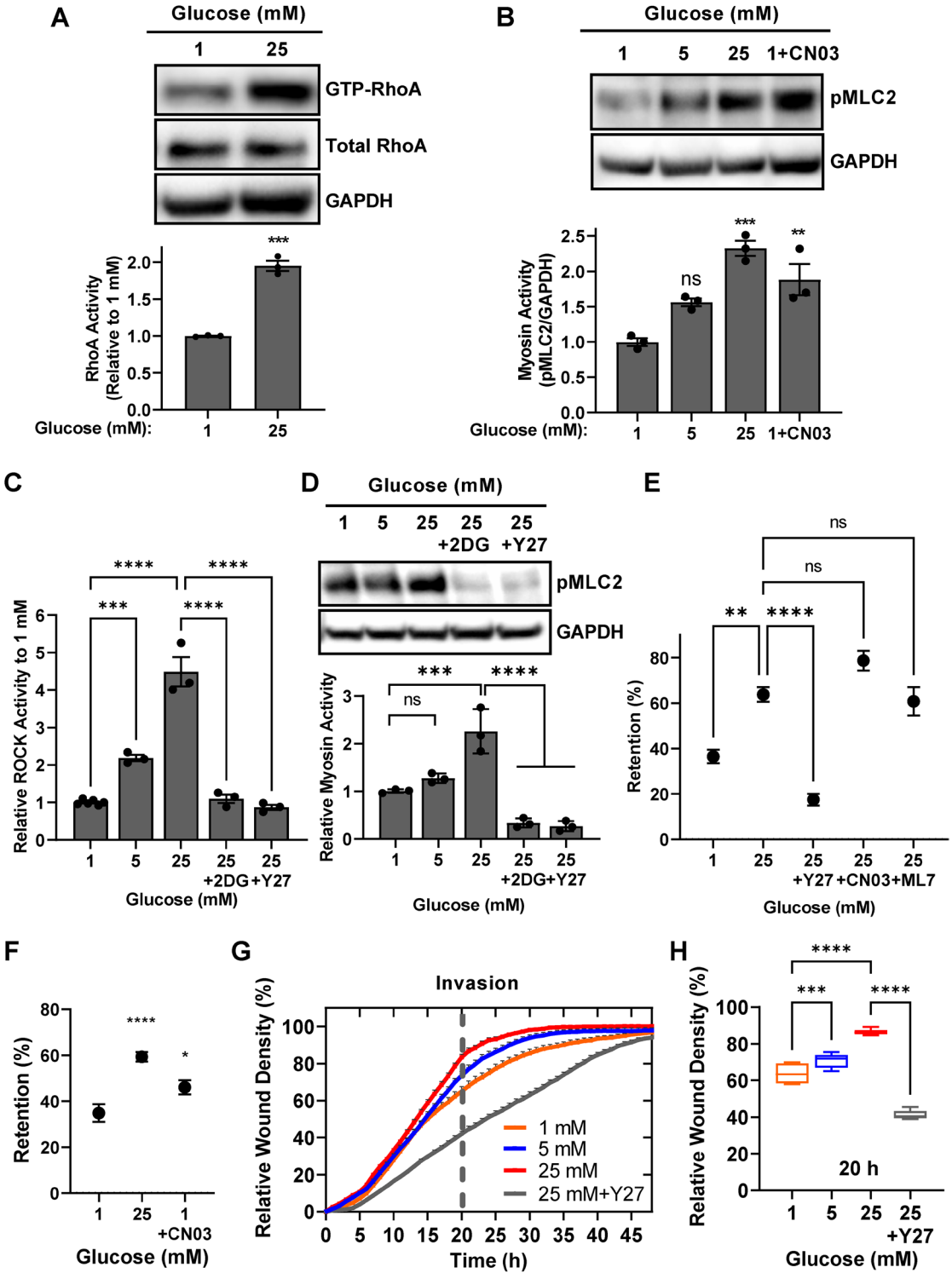

FIGURE 5: RhoA-ROCK signaling axis is activated with high-glucose treatment in MDA-MB-231 cells. (A) RhoA activity measured by GTP-RhoA pull-down assay with high-glucose treatment. Quantitation of the total and active RhoA protein is normalized to 1 mM glucose treatment (below panel). Statistical significance was determined by unpaired *t* test ($n = 3$). (B) pMLC2 levels after glucose or Rho activator (CN03) treatment for 3 h. Quantitation is shown below ($n = 3$). (C) Kinase activity of ROCK measured by an enzyme-based immunoassay after glucose, glycolysis inhibitor (2DG), or ROCK inhibitor (Y27632) treatment for 3 h ($n = 3$). Normalized to 1-mM treatment. (D) pMLC2 levels after glucose or inhibitors treatment for 3 h. Normalized to 1-mM treatment. Quantitation is shown below ($n = 3$). (E) Whole-cell deformability measured by PMF after glucose, CN03, or inhibitors treatment (ML7: MLCK inhibitor; $n = 3$). (F) Whole-cell deformability measured by PMF after glucose or Rho activator treatment for 3 h ($n = 3$). (G) Relative wound density as a function of time from the scratch wound invasion assay. The dashed gray line indicates the time point (20 h) that is shown in (H) ($n = 8$). All error bars represent mean ± SEM. Unless otherwise stated, statistical significance was determined by one-way ANOVA test (ns, not significant; *, $p < 0.05$; **, $p < 0.01$; ***, $p < 0.001$; ****, $p < 0.0001$).

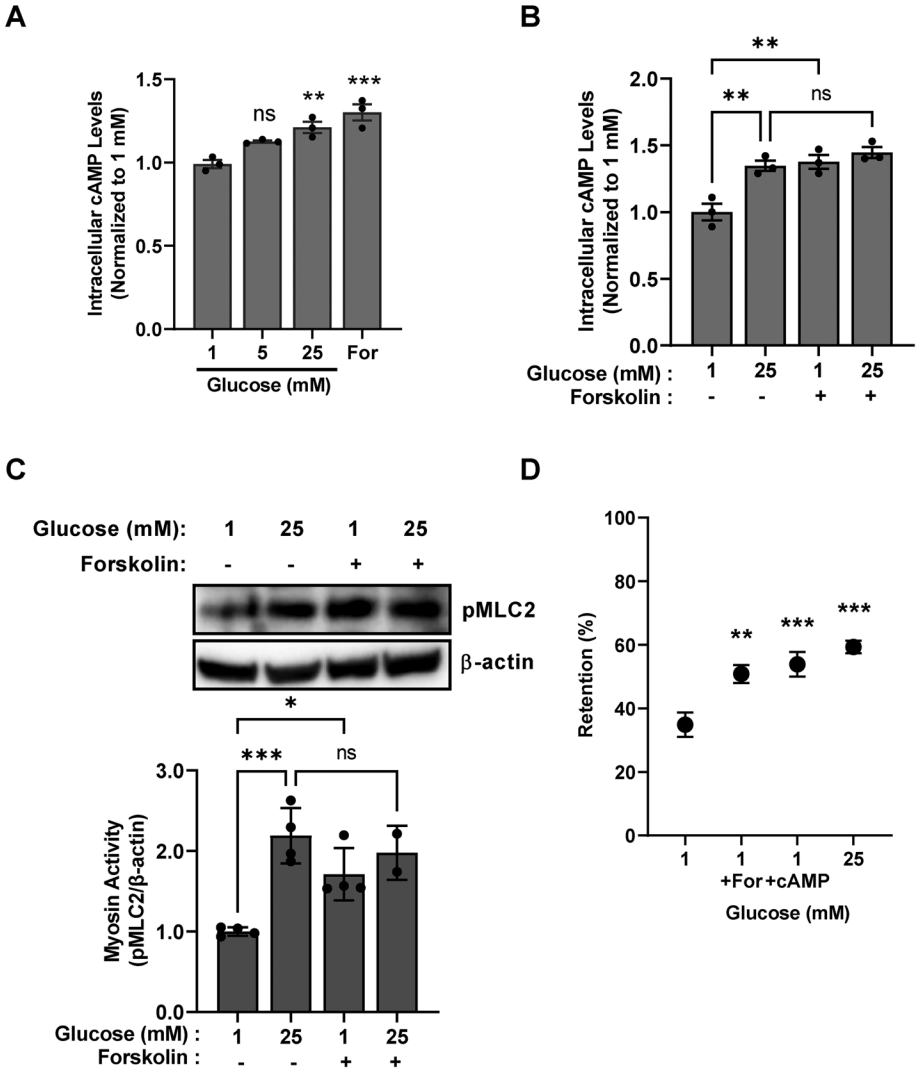

FIGURE 6: cAMP mediates glucose-induced cell mechanotype changes. (A) Intracellular cAMP levels measured by competitive ELISA assay after treatment with different glucose concentrations. Forskolin (For, 10 μM) was used as a positive control to increase intracellular cAMP levels. All comparisons were made to 1-mM glucose treatment ($n = 3$). (B) Intracellular cAMP levels in MDA-MB-231 cells treated with different glucose concentrations with or without forskolin. All comparisons were made to 1-mM glucose treatment ($n = 3$). (C) pMLC2 levels in MDA-MB-231 cells treated with different glucose concentrations with or without forskolin. Quantitation is shown below ($n = 4$). (D) Whole-cell deformability was measured after treatment with forskolin and cAMP analog for 3 h under low glucose conditions ($n = 3$). All error bars represent mean ± SEM. All statistical significance was determined by one-way ANOVA test (ns, not significant; *, $p < 0.05$; **, $p < 0.01$; ***, $p < 0.001$; ****, $p < 0.0001$).

cell mechanotype, we measured intracellular cAMP levels in high glucose–treated MDA-MB-231 cells. After high-glucose treatment for 3 h, we observed a significant increase in intracellular cAMP levels, similar to that for forskolin treatment, which activates adenylyl cyclases (ACs) to raise cAMP levels (Pinto *et al.*, 2008; Figure 6A). Additional forskolin treatment in high glucose–treated cells had no additive effect on cAMP production, while forskolin treatment in low glucose–treated cells significantly increased cAMP levels (Figure 6B). This suggests that the signaling pathway activated by high-glucose treatment shares the same ACs, which are activated by forskolin. Forskolin treatment also increased myosin activity (Figure 6C) similarly to high-glucose treatment, suggesting that cAMP signaling is involved in myosin activation. Consistent with our high glucose–induced cell deformability change data (Figure 1C), increase in intracellular cAMP level either by forskolin treatment or by treatment with 8-bromoadenosine 3′,5′-cyclic adenosine monophosphate (8-Br-cAMP), a cell-permeable cAMP analog, significantly reduced cell deformability under low-glucose conditions (Figure 6D). Because cAMP increased myosin activity and decreases whole cell deformability, we further asked whether cAMP activates the RhoA-ROCK axis. Forskolin treatment undern low-glucose conditions resulted in about a 1.9-fold increase in RhoA activity (Figure 7A), suggesting that cAMP is a bona fide mediator that translates a high-glucose signal into activation of the RhoA-ROCK axis. We also observed that ROCK, but not MLCK or PAK1, is required for forskolin-induced myosin activation (Figure 7B). In addition, other studies have reported that cAMP signaling regulates cell migration by controlling the dynamics of actin cytoskeleton rearrangement (Lorenowicz *et al.*, 2007; Borland *et al.*, 2009; Kim *et al.*, 2015). Consistent with these studies, we observed that forskolin treatment increased F-actin levels similarly to the increase in F-actin levels in high glucose–treated MDA-MB-231 cells (Figure 7, C and D). To confirm the forskolin-induced F-actin increase is due to increased intracellular cAMP level, we treated the cells with 8-Br-cAMP. Cells treated with 8-Br-cAMP also showed increased F-actin levels (Figure 7E) consistent with the F-actin modulation function of cAMP in mouse embryonic stem cells (Kim *et al.*, 2015). Because ROCK stabilizes F-actin and actomyosin stress fibers (Guerra *et al.*, 2017; Chen *et al.*, 2020), we asked if the increased F-actin level by cAMP is ROCK-dependent. The increased F-actin level by forskolin was not changed after ROCK inhibition with Y27632 (Figure 7F). Consistently, we observed that when colocalization of F-actin and active myosin was disorganized by ROCK inhibition with Y27632, the level of F-actin remained high (Figure 7, G and H). Taken together, our results suggest that an increased intracellular cAMP level can increase the level of F-actin independent of ROCK.

DISCUSSION

During early metastasis, cancer cells experience a variety of soluble cues such as oxygen, hormones, and glucose at a wide range of concentrations. These soluble cues may act as regulators of cellular mechanical properties in cancer cells. Previously, we have reported that activation of βAR signaling increases cell stiffness and contractility (Kim *et al.*, 2016). Similarly, others have reported that TGF-β signaling increases cellular stiffness and invasiveness in lung cancer cells (Gladilin *et al.*, 2019). In this study, we investigated the effect of high glucose levels on cell mechanotypes and motility. Because

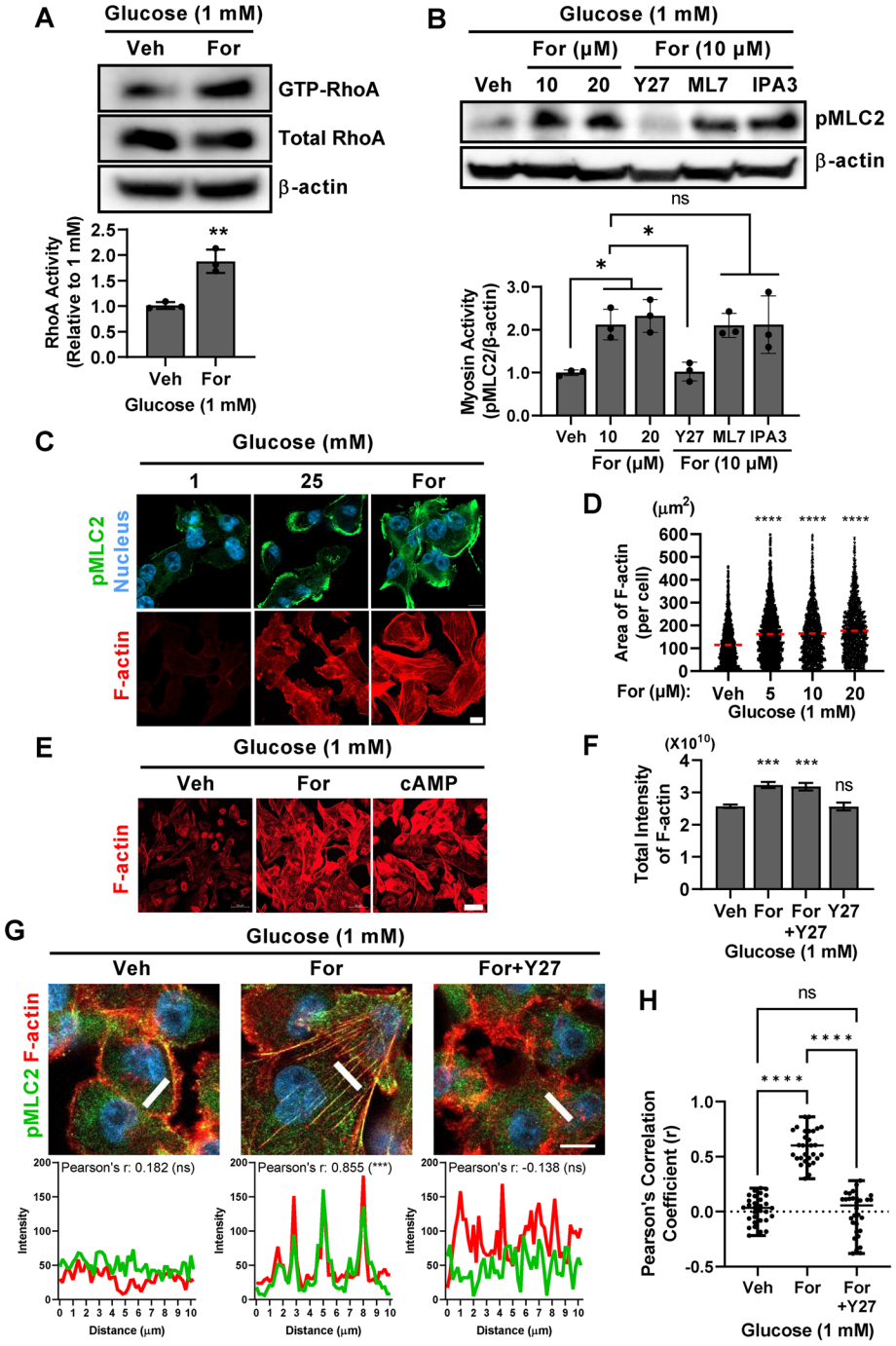

FIGURE 7: cAMP increases cell stiffness through activating RhoA-ROCK-NMII axis and increases actomyosin filament. (A) RhoA activity measured by GTP-RhoA pull-down assay with forskolin treatment. Quantitation of the total and active RhoA protein is normalized to vehicle treatment (below panel). Statistical significance was determined by unpaired *t* test ($n = 3$). (B) pMLC2 levels after forskolin treatment for 3 h with or without inhibitors for ROCK (Y27), MLCK (ML7), or PAK1 (IPA3). Quantitation is shown below ($n = 3$). (C) Representative confocal microscopy images of pMLC2 (green) and F-actin (red) from MDA-MB-231 cells treated with glucose or forskolin for 3 h. Scale bar, 10 μm. (D) Quantification of F-actin area per cell with increasing concentration of forskolin analyzed by Cellinsight CX7 HCA system ($n = 3$; 24 h). (E) Representative confocal microscopy images of F-actin from MDA-MB-231 cells treated with forskolin or cAMP analog for 24 h. Scale bar, 50 μm. (F) Total F-actin intensity per well measured from MDA-MB-231 cells treated with forskolin with or without Y27632 for 24 h ($n = 8$). (G) Subcellular localization of pMLC2 (green) and F-actin (red). Fluorescence intensity of each target in a marked region (white line) was analyzed using line intensity profiles (below each image). Pearson's correlation coefficient representing colocalization efficiency is denoted. Scale bar, 10 μm (3 h). (H) Comparison of Pearson's correlation coefficient (*r*) values from randomly selected marked regions ($n = 30$). All error bars represent mean ± SEM. Unless otherwise stated, statistical significance was determined by one-way ANOVA test (ns, not significant; *, $p < 0.05$; **, $p < 0.01$; ***, $p < 0.001$; ****, $p < 0.0001$).

cytoskeletal remodeling during cell invasion requires high energy expenditure, cells, especially cancer cells, depend on glucose uptake as their primary fuel source. Tumor tissues have 13 to 45 times less glucose than normal counterpart tissues (Hirayama *et al.*, 2009). During early metastasis, therefore, cancer cells travel from glucose-depleted regions within the tumor microenvironment to glucose-rich regions in surrounding tissues. Because peripheral tissues have lower glucose levels than blood, cancer cells experience even higher glucose levels when they enter into blood circulation (Hirayama *et al.*, 2009). Despite the important role of glucose in cell physiology and pathogenesis, its impact on cell mechanotype has not been investigated well. Considering that cell mechanotype regulates cell invasion and other functions, it is critical to understand how increased extracellular glucose levels modulate cell mechanotype and function. Here, we report for the first time that high glucose levels increase breast cancer cell stiffness and contractility, which are associated with increased cell motility through the cAMP-RhoA-ROCK-NMII axis (Figure 8).

In previous works, we discovered that activation of βAR signaling, which raises intracellular cAMP level, increases cell stiffness and contractility (Kim *et al.*, 2016). In the current study, we show that high extracellular glucose levels increase glycolysis and intracellular cAMP levels, which results in increased cell stiffness and contractility in breast cancer cells. Collectively, these data suggest that cAMP may play a central role in translating extracellular signaling cues into cell mechanotype changes, although in a cell type–specific manner. Here we show that increased cAMP levels activate the RhoA-ROCK-NMII axis and increase actomyosin stress fibers in a ROCK–dependent manner in MDA-MB-231 cells. However, there is a contradictory study reporting that cAMP inhibits RhoA activity in rat cardiac fibroblasts (Oishi *et al.*, 2012). Similarly, another study has shown that cAMP reduces MLCK activity by hindering its interaction with Ca^{2+}/calmodulin in mouse arteries (Raina *et al.*, 2009), yet no difference in MLCK activity with high glucose that increases cAMP level was observed here. This suggests that cAMP may regulate cell

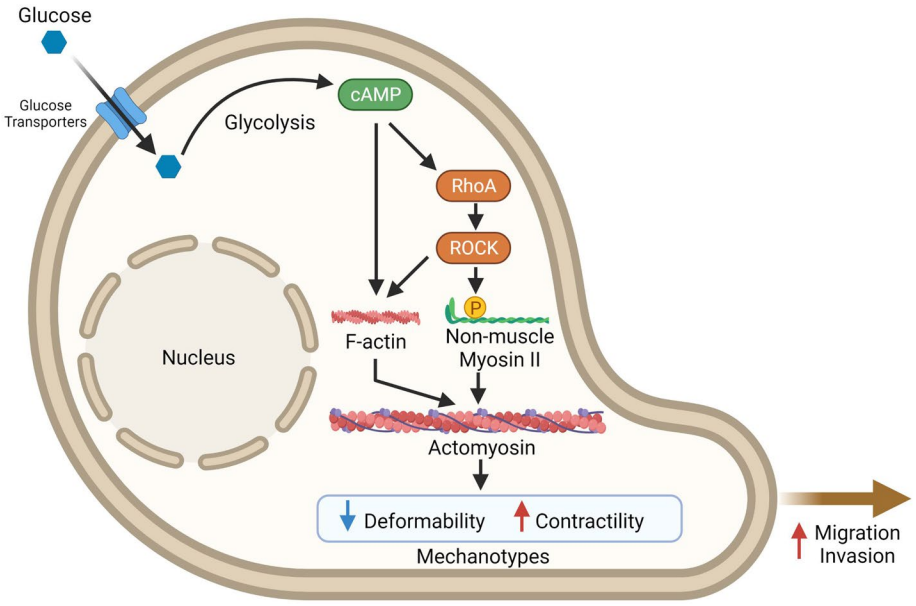

FIGURE 8: Schematic illustration of proposed model. Proposed mechanism for glucose regulation of breast cancer cell mechanotype and motility. Glucose taken by a cell enters into glycolysis metabolic pathway, resulting in increase of intracellular cAMP level. cAMP signaling increases F-actin levels and activates RhoA-ROCK-NMII axis, which results in decreased cell deformability and increased contractility. These altered mechanotype also correlates with increased cell migration and invasion. Created with BioRender.com.

motility in a cancer type–specific manner as well. Although cAMP suppressed motility of pancreatic cancer cells (Zimmerman *et al.*, 2015), cAMP has promigration and proinvasion effects in most cancer types (Zhang *et al.*, 2020). Therefore, further studies are needed to elucidate the detailed molecular mechanisms by which cAMP regulates RhoA and MLCK in a cell type– and/or cancer type–dependent manner.

In this study, high glucose–induced cell mechanotype changes were observed as early as 3 h after glucose treatment. Because myosin activity and F-actin rearrangement contribute to cell mechanotype changes, our data suggest that the altered mechanotype can be sustained up to 24 h in our experimental system. This may partially explain the increased cell migration and invasion at later time points at 48 or 72 h, although it is still unclear how the cell mechanotype changes dynamically over time at the transcriptional and posttranscriptional level. Further studies are needed to determine the duration and reversibility of F-actin rearrangement and myosin activation. We speculate that they will fluctuate over time at late time points (>24 h) by feedback mechanisms of signaling molecules. For example, intracellular cAMP levels are regulated by ACs and phosphodiesterases (PDEs; Sassone-Corsi, 2012). Because cAMP is a ubiquitous second messenger and central regulator of diverse cellular functions, spatiotemporal regulation of cAMP is critical for cells to ensure specificity in cAMP signaling (Hayes *et al.*, 1980; Brunton *et al.*, 1981). An existing Förster resonance energy transfer (FRET) sensor for detection of cAMP dynamics (Surdo *et al.*, 2017) will be useful to correlate the cAMP levels and cell mechanotype changes over time in future studies.

Because MDA-MB-231/HM cells are a highly metastatic variant of MDA-MB-231 cells, we expected that MDA-MB-231/HM cells will show faster migration and invasion than MDA-MB-231 cells. Interestingly, however, we observed that MDA-MB-231/HM cells show slower invasion than MDA-MB-231 cells, while MDA-MB-231/HM cells show faster migration than MDA-MB-231 cells (Supplemental Figure S4, C and D). This unexpected result may stem from the difference in basal levels of F-actin and MLC2 between the two cell types. MDA-MB-231/HM cells have significantly higher F-actin levels than MDA-MB-231 cells (Supplemental Figure S4F) despite the similar β-actin mRNA levels (Supplemental Figure S4E). In contrast, MDA-MB-231/HM cells have significantly lower basal MLC2 expression levels than MDA-MB-231 cells in both protein (Supplemental Figure S4H) and mRNA (Supplemental Figure S4G) levels. Further studies are needed to elucidate whether the differential basal levels of F-actin and MLC2 contribute to the lower invasion rate of MDA-MB-231/HM cells than of MDA-MB-231 cells. Nevertheless, other factors such as cell adhesion and/or secretion of extracellular matrix–degrading enzymes may also contribute to the cell motility.

We have shown that high extracellular glucose levels increase glycolysis rate and intracellular cAMP levels, as well as inducing increased activation of the RhoA-ROCK-NMII axis. However, the molecular link between increased glycolysis rate and cAMP production is unknown. We speculate that glycolysis mediators such as metabolites and metabolic enzymes may activate ACs or inhibit PDEs, although further investigation is required. Our measurement of *ADCYs* mRNA expression levels, which encode ACs (Supplemental Figure S7A), was consistent with a previous report (Guo *et al.*, 2022). Because *ADCY3, 6, 7,* and *9* are differentially expressed in MDA-MB-231 cells and in MDA-MB-231/HM and MCF7 cells (Supplemental Figure S7, B–E), future studies will investigate the role of these *ADCY* isoforms in translating high–extracellular glucose signals into cAMP production. Additionally, the mechanisms by which increased cAMP levels activate the RhoA-ROCK signaling pathways have yet to be elucidated. Multiple effector proteins are reported that relay cAMP signals: cAMP-dependent protein kinase (PKA), exchange protein activated by cAMP (Epac), cAMP-gated channel (CNGC), and the Popeye domain–containing (POPDC) protein family (Kopperud *et al.*, 2003; Brand and Schindler, 2017). Currently such cAMP effector proteins are under investigation to identify the molecules involved in high glucose-induced RhoA activation in breast cancer cells.

Recent studies have shown increased breast cancer-specific death in obese breast cancer patients (Protani *et al.*, 2010; Chan *et al.*, 2014; Blair *et al.*, 2019). Because obesity is accompanied by hyperglycemia, we hypothesized that high extracellular-glucose levels modulate cancer cell mechanotype and motility, which may promote cancer metastasis. For the first time, to our best knowledge, we report here that high extracellular-glucose levels alter the mechanotype of TNBC cells through the cAMP-RhoA-ROCK-NMII axis, which is also associated with increased cell migration and invasion in vitro. Future in vivo studies to further elucidate the molecular pathways regulating the cAMP-RhoA-ROCK-NMII axis in the context of various extracellular glucose levels will improve our understanding of the link between obesity and tumor metastasis, and ultimately will provide a foundation for the identification of novel drug targets for the prevention of metastasis in TNBC.

MATERIALS AND METHODS

Request a protocol through *Bio-protocol*.

Cell culture and chemicals

MCF7 and MDA-MB-231 human breast cancer cell lines and the highly metastatic variant of MDA-MB-231, MDA-MB-231/HM (a kind gift from Zhou Ou, Fudan University Shanghai Cancer Center; Chang *et al.*, 2008), were cultured in DMEM supplemented with 10% fetal bovine serum (FBS) and 1% penicillin/streptomycin. The MCF10A cell line was cultured in DMEM/Ham's F12 nutrient mixture (DMEM/F12) supplemented with 10 µg/ml insulin, 20 ng/ml EGF, 100 ng/ml cholera toxin, 0.5 µg/ml hydrocortisone, 5% horse serum, and 100 U/ml penicillin/streptomycin. For the glucose treatment experiment with MCF10A cells, glucose-free DMEM/F12 media (Elabscience) was supplemented with desired glucose concentrations. Cells were maintained at 37°C with 5% CO_2 in a humidified incubator. All cell culture materials were purchased from GIBCO. Prior to D-glucose (GIBCO) treatment, cells were cultured for 48 h in a culture medium containing 5 mM glucose to exhaust extracellular glucose levels (Supplemental Figure S1A). Glucose-starved cells were then treated with different concentrations of D-glucose (1, 5, 11, or 25 mM) for 3 or 24 h followed by downstream assays. The osmolarity in low glucose media was maintained by complementing D-mannitol (GIBCO) to the culture medium to make 25 mM in total. Pharmacological inhibitors and activators were purchased from commercial vendors as following: Rho-associated kinase (ROCK) inhibitor, Y27632 (Selleck Chemicals, S6390), myosin light-chain kinase (MLCK) inhibitor, ML-7 (Selleck Chemicals, S8388), glycolysis inhibitor, 2-deoxy-D-glucose (2DG) (Sigma-Aldrich, D8375), p21-activated kinase 1 (PAK1) inhibitor, IPA3 (Selleck Chemicals, S7093), Rho activator II, CN03 (Cytoskeleton, CN03), adenyl cyclase activator, Forskolin (Selleck Chemicals, S2449), and cAMP Analog, 8-Br-cAMP (Selleck Chemicals, S7857). Cells were treated with 2DG at 25 mM, 8-Br-cAMP at 100 µM, and all other drugs at 10 µM for indicated time.

Parallel microfiltration assay

To measure whole cell deformability, we used parallel microfiltration (PMF; Qi *et al.*, 2015). Cells treated with different glucose concentrations for 3 h were trypsinized with 0.05% trypsin–EDTA and cells in suspension were counted using an automated cell counter (Corning Cell Counter, CytoSMART) and resuspended in culture medium to a density of 5×10^5 cells/ml. We also used the automated cell counter to measure cell size distributions. No significant changes in cell size distribution was observed after different glucose and/or inhibitors treatment (Supplemental Figure S2A). To allow cells to equilibrate after lifting into suspension, suspensions were maintained for 30 min before filtration. To drive cells through the 8-µm pores of the polycarbonate membrane (Sterlitech), we applied air pressure (5.5 kPa) for 60-120 s. To quantify the magnitude of cell filtration, we determined the volume of media that remained in the top well after filtration by measuring absorbance at $\lambda_{560\ nm}$ using a microplate reader (Synergy HTX, BioTek; Gill *et al.*, 2019). Cells with reduced deformability have a higher probability of occluding pores and consequently exhibit a higher retention of fluid in the top well; we define the final volume of media retained in the top well compared with the initial volume loaded, $Vol_{final}/Vol_{initial}$, as % retention.

Single-cell contractility assay

Single-cell contraction was measured using fluorescent elastomeric contractible surfaces (FLECS) technology (Forcyte Biotechnologies). The FLECS plate was patterned with a uniform shape composed of collagen and fluorescent fibrinogen on soft elastomer films (Pushkarsky *et al.*, 2018). In each well, 5000 cells were seeded on the 96-well FLECS plate and cells were adhered to micropatterns for 24 h in the growth medium with 1 mM glucose. Cells were then treated with different concentrations of D-glucose for 3 h, followed by staining with Hoechst 33342 (Thermo Fisher Scientific) for 5 m. Only micropatterns with a single cell attached were selected for analysis. To measure the degree of single-cell contraction, high-resolution images of micropatterns were obtained using an LSM 900 scanning confocal microscope (Carl Zeiss, Oberkochen, Germany), and the pixel areas of micropatterns were analyzed using the ZEN image analysis program (ZEN3.4, Carl Zeiss).

Immunoblotting

For Western blotting, total protein was prepared by lysing cells for 30 min on ice with ice-cold RIPA buffer (Thermo Fisher Scientific) containing protease and phosphatase inhibitor cocktails (Thermo Fisher Scientific). After centrifugation of the lysates at 13,000 rpm for 15 min at 4°C, the concentration of total soluble proteins in supernatant was measured using a BCA protein assay kit (Thermo Fisher Scientific). The same amount of total proteins throughout samples was prepared followed by boiling the lysates with LDS sample buffer (NOVEX) containing 100 mM of dithiothreitol (DTT; Cell Signaling Technology) for 5 min. For SDS–PAGE, 4–12% gradient Bolt gels (Thermo Fisher Scientific) were used with MES SDS running buffer (Thermo Fisher Scientific). Protein samples were transferred onto a methanol-activated polyvinylidene difluoride (PVDF) membrane with pore size 0.45 µm (Thermo Fisher Scientific). The membrane was blocked with SuperBlock T20 blocking buffer (Thermo Fisher Scientific) at room temperature for 1 h and incubated with primary and secondary antibodies as follows: for primary antibodies, p-MLC2 (Ser19; Cell Signaling Technology, 3671) 1:1000 dilution, p-MLCK (Ser1760; Invitrogen, 44-1085G) 1:1000 dilution, GAPDH (Invitrogen, MA5-15738) 1:1000 dilution, and β-actin (Invitrogen, MA5-15739) 1:3000 dilution at 4°C overnight. For secondary antibodies, goat anti-rabbit-IgG conjugated to horseradish peroxidase (HRP; Santa Cruz Biotechnology, SC-2387) 1:5000 dilution and goat anti-mouse-IgG conjugated to HRP (Santa Cruz Biotechnology, SC-516102) 1:5000 dilution at room temperature for 1 h. For signal development, we used ECL or Pico SuperSignal chemiluminescent substrate (Thermo Fisher Scientific) according to the manufacturer's protocol. For protein quantification, images were acquired using ChemiDoc XRS (Biorad) and band intensity was analyzed using Image Lab software (BioRad).

Immunocytochemistry

For immunocytochemistry, 30,000 cells were seeded in a four-well chamber (Thermo Fisher Scientific) and treated with glucose as described above. After fixation with 4% paraformaldehyde for 15 min at room temperature, cells were blocked with blocking buffer (Cell Signaling Technology) for 60 min at room temperature. Then cells were incubated with p-MLC2 antibody (Cell Signaling Technology, 3671) diluted 1:50 overnight at 4°C. Secondary antibody conjugated with Alexa Fluor 488 (Molecular Probes, R37116) was used for visualization. For costaining with filamentous actin (F-actin), cells were stained with Acti-stain 555 phalloidin (Cytoskeleton, PHDH1) as described in the manufacturer's instructions. Then DAPI (Invitrogen, R73606) was added for nucleus staining. Confocal microscopy images were acquired using LSM900 scanning microscope (Carl Zeiss) equipped with 63×, 40×, and 20× magnification objectives. To determine subcellular localization of

pMLC2 and F-actin, confocal microscopy images were analyzed with line profiles using ZEN 3.4 software (Carl Zeiss). The colocalization of pMLC2 and F-actin signals was evaluated with Pearson's correlation coefficient (*r*).

Quantitative analysis of F-actin

To analyze F-actin levels quantitively, we used two methods, confocal microscopy and Cellinsight High-Content Analysis, to acquire and analyze F-actin-stained cell images. For confocal microscopy, 30,000 or 10,000 cells were seeded in a four-well chamber or an optical 96-well plate, respectively. After overnight incubation, cells were treated with glucose as described above. F-actin was stained with Acti-stain 488/555 phalloidin (Cytoskeleton, PHDG1/PHDH1) for fixed cells or an SiR-actin probe for live cells as described in the manufacturer's instructions (Cytoskeleton, CY-SC001). DAPI or Hoechst 33342 (Invitrogen) was added for nucleus staining. Representative confocal microscopy images were acquired using an LSM900 scanning microscope (Carl Zeiss). For quantification of F-actin levels, confocal microscopy images were randomly captured with a 20× objective and the total fluorescence intensity from only the area covered by cells from each image was quantified using ZEN 3.4 software (Carl Zeiss) and normalized to the number of nuclei. For unbiased quantification of F-actin levels as an independent validation, we used a High-Content Analysis (HCA) system (Cellinsight CX7, Thermo Fisher Scientific). Nine images were acquired with a 10× objective from each well. F-actin quantitation was computed using a dedicated proprietary algorithm (Cellomics Target Activation V4).

Cell migration and invasion assay

To measure collective cell migration in real time, we used the Incucyte scratch wound healing assay (Essen BioScience). In each well of an ImageLock 96-well plate (Essen BioScience), 5×10^4 cells were seeded and incubated for 24 h to form a confluent cell monolayer. A scratch wound was made using WoundMaker (Essen BioScience) and images were acquired every 1 h. The relative wound density was calculated using IncuCyte ZOOM (ver. 2018A) software (Essen BioScience). For cell invasion assay, the ImageLock 96-well plate was precoated with 100 µg/ml Cultrex BME extract (R&D systems) and 5×10^4 cells were plated in each well. After 24 h, scratch wound was introduced as described above and 2 mg/ml Cultrex was added to cover the entire well.

Real-time cell metabolic analysis

An XF-e96 extracellular flux analyzer (Seahorse Bioscience) was used for real-time analysis of extracellular acidification rate (ECAR) and oxygen consumption rate (OCR) in cells treated with different glucose concentrations. Cells were grown on Seahorse cell culture microplates with 5-mM glucose medium for 3 days. The glucose-starved cells were washed with XF assay medium (Seahorse Bioscience) containing 1-mM glucose (pH adjusted to 7.4) and equilibrated for 1 h in the Seahorse incubator. The XF96 plate was inserted into the Seahorse analyzer, where 10 basal assay cycles were performed, consisting of 3 min of mixing followed by 3 min of measuring. After completion of the basal level measurement, different concentrations of glucose were added by automatic pneumatic injection port, and measurements were performed for 100 assay cycles. ECAR and OCR values were normalized to the baseline measurements. Cell numbers in each well were obtained using Cytation 1 (Agilent) to normalize the ECAR and OCR values. Measurements were performed in six replicates (six wells) for each independent experiment.

Measurement of Ca^{2+} concentration

Intracellular calcium ion concentrations were measured using a colorimetric calcium assay kit (Abcam) as instructed by the manufacturer. Briefly, 5×10^5 cells were plated in 100-mm cell culture dishes and treated with different concentrations of glucose as described above. After glucose treatment, cells were lysed with RIPA buffer without EDTA, and 50 µl of the lysate was used for calcium analysis. Free calcium ions form a chromogenic complex with o-cresolphthalein that can be measured at absorbance 575 nm using a microplate reader (Synergy HTX, BioTek).

RhoA activation assay

The RhoA activation assay was performed using a RhoA Pull-down Activation Assay Biochem kit (Cytoskeleton). Cells were treated with each glucose concentration for 5 min and snap-freezing for analysis of RhoA activation. Then 500–800 µg of cellular extract was immunoprecipitated with Rhotekin-RBD beads according to the manufacturer's instructions. Total and active RhoA protein were quantified using ImageLab software (BioRad). The ratio of active to total RhoA was compared between 1- and 25-mM glucose-treated cells using densitometric data.

Measurement of ROCK activity

ROCK activity was measured by enzyme immunoassay using a ROCK activity assay kit (Cell Biolabs) as instructed by the manufacturer. Briefly, 200 µg of total protein was added to each well of the assay plate, where the ROCK substrate, MYPT1, was coated. After 60 min incubation at 30°C for the kinase reaction, the plate was incubated with anti-phospho-MYPT1 (Thr696) antibody, followed by incubation with HRP-labeled secondary antibody. The ROCK kinase activity was determined by quantification of color development at absorbance 450 nm using a microplate reader (Synergy HTX, BioTek).

Measurement of cyclic adenosine monophosphate (cAMP)

Intracellular cAMP levels were measured using the cAMP Competitive ELISA kit (Abcam) according to the manufacturer's protocol. Briefly, cell lysates with 100 µg total protein were loaded into wells coated with anti-cAMP antibody. HRP-labeled cAMP is also added to the wells to compete with intracellular cAMP for the fixed number of anti-cAMP antibody binding sites on the plate. After washing out unbound cAMP molecules, the amount of bound HRP-labeled cAMP was measured using a fluorometric HRP substrate.

Statistical analysis

All experiments were performed at least three independent times for reproducibility. Statistical significance between control and treated groups was determined with an unpaired *t* test or one-way ANOVA with Dunnett's multiple comparison post hoc analysis using GraphPad Prism 9 (GraphPad Software, La Jolla, CA). Total numbers of data points from technical replicates for statistical test are denoted by "*n*" in figure legends. To determine statistically significant differences between cell size distributions, we used Kruskal–Wallis one-way ANOVA with Dunnett's multiple comparison post hoc analysis. The following *p* values were considered to be statistically significant: p value ≤ 0.05 (*), p value ≤ 0.01 (**), and p value ≤ 0.001 (***).

ACKNOWLEDGMENTS

The authors thank Helen Hathaway for helping us to use their Incucyte equipment. The authors also thank the IDeA National Resource

for Quantitative Proteomics, funded by a grant from the National Institute of General Medical Sciences (R24GM137786), for data acquisition and data analysis. Confocal microscopy and flow cytometry analyses were performed in the UNM Comprehensive Cancer Center Shared Resources, which are supported by a UNM Comprehensive Cancer Center Support Grant (NCI P30CA118100). Seahorse real-time cell metabolic analysis and Cellomics High-Content Analysis were performed in the UNM AIM Center Core Facility, which is funded by a NIH/NIGMS Grant (P20GM121176). This work was supported by NIH Grants P30CA118100 (UPN fellow to S.B.) and P20GM121176 (mPI to T.-H.K.), a UNM Department of Pathology start-up fund to T.-H.K., and a METAvivor Early Career Investigator Award to T.-H.K.

REFERENCES

Aoun R, El Hadi C, Tahtouh R, El Habre R, Hilal G (2022). Microarray analysis of breast cancer gene expression profiling in response to 2-deoxyglucose, metformin, and glucose starvation. Cancer Cell Int 22, 123.

Bhardwaj P, Brown KA (2021). Obese adipose tissue as a driver of breast cancer growth and development: update and emerging evidence. Front Oncol 11, 638918.

Blair CK, Wiggins CL, Nibbe AM, Storlie CB, Prossnitz ER, Royce M, Lomo LC, Hill DA (2019). Obesity and survival among a cohort of breast cancer patients is partially mediated by tumor characteristics. NPJ Breast Cancer 5, 33.

Blanchoin L, Boujemaa-Paterski R, Sykes C, Plastino J (2014). Actin dynamics, architecture, and mechanics in cell motility. Physiol Rev 94, 235–263.

Borland G, Smith BO, Yarwood SJ (2009). EPAC proteins transduce diverse cellular actions of cAMP. Br J Pharmacol 158, 70–86.

Brand T, Schindler R (2017). New kids on the block: the Popeye domain containing (POPDC) protein family acting as a novel class of cAMP effector proteins in striated muscle. Cell Signal 40, 156–165.

Brown GK (2000). Glucose transporters: structure, function and consequences of deficiency. J Inherit Metab Dis 23, 237–246.

Brunton LL, Hayes JS, Mayer SE (1981). Functional compartmentation of cyclic AMP and protein kinase in heart. Adv Cyclic Nucleotide Res 14, 391–397.

Carey LA, Dees EC, Sawyer L, Gatti L, Moore DT, Collichio F, Ollila DW, Sartor CI, Graham ML, Perou CM (2007). The triple negative paradox: primary tumor chemosensitivity of breast cancer subtypes. Clin Cancer Res 13, 2329–2334.

Chan DSM, Vieira AR, Aune D, Bandera EV, Greenwood DC, McTiernan A, Navarro Rosenblatt D, Thune I, Vieira R, Norat T (2014). Body mass index and survival in women with breast cancer—systematic literature review and meta-analysis of 82 follow-up studies. Ann Oncol 25, 1901–1914.

Chang XZ, Li DQ, Hou YF, Wu J, Lu JS, Di GH, Jin W, Ou ZL, Shen ZZ, Shao ZM (2008). Identification of the functional role of AF1Q in the progression of breast cancer. Breast Cancer Res Treat 111, 65–78.

Chen MC, Hsu LL, Wang SF, Hsu CY, Lee HC, Tseng LM (2020). ROS mediate xCT-dependent cell death in human breast cancer cells under glucose deprivation. Cells 9, 1598.

Choi J, Cha YJ, Koo JS (2018). Adipocyte biology in breast cancer: from silent bystander to active facilitator. Prog Lipid Res 69, 11–20.

Ekpenyong AE, Whyte G, Chalut K, Pagliara S, Lautenschläger F, Fiddler C, Paschke S, Keyser UF, Chilvers ER, Guck J (2012). Viscoelastic properties of differentiating blood cells are fate- and function-dependent. PLoS One 7, e45237.

Flatau G, Lemichez E, Gauthier M, Chardin P, Paris S, Fiorentini C, Boquet P (1997). Toxin-induced activation of the G protein p21 Rho by deamidation of glutamine. Nature 387, 729–733.

Follain G, Herrmann D, Harlepp S, Hyenne V, Osmani N, Warren SC, Timpson P, Goetz JG (2020). Fluids and their mechanics in tumour transit: shaping metastasis. Nat Rev Cancer 20, 107–124.

Fujita M, Imadome K, Somasundaram V, Kawanishi M, Karasawa K, Wink DA (2020). Metabolic characterization of aggressive breast cancer cells exhibiting invasive phenotype: impact of non-cytotoxic doses of 2-DG on diminishing invasiveness. BMC Cancer 20, 929.

Garrido P, Osorio FG, Morán J, Cabello E, Alonso A, Freije JM, González C (2015). Loss of GLUT4 induces metabolic reprogramming and impairs viability of breast cancer cells. J Cell Physiol 230, 191–198.

Gill NK, Ly C, Nyberg KD, Lee L, Qi D, ToFigure B, Reis-Sobreiro M, Dorigo O, Rao J, Wiedemeyer R, *et al.* (2019). A scalable filtration method for high throughput screening based on cell deformability. Lab Chip 19, 343–357.

Giovannucci E, Harlan DM, Archer MC, Bergenstal RM, Gapstur SM, Habel LA, Pollak M, Regensteiner JG, Yee D (2010). Diabetes and cancer: a consensus report. Diabetes Care 33, 1674–1685.

Gladilin E, Ohse S, Boerries M, Busch H, Xu C, Schneider M, Meister M, Eils R (2019). TGFβ-induced cytoskeletal remodeling mediates elevation of cell stiffness and invasiveness in NSCLC. Sci Rep 9, 7667.

Gorovits N, Charron MJ (2003). What we know about facilitative glucose transporters: lessons from cultured cells, animal models, and human studies. Biochemistry and Molecular Biology Education 31, 163–172.

Grover-McKay M, Walsh SA, Seftor EA, Thomas PA, Hendrix MJ (1998). Role for glucose transporter 1 protein in human breast cancer. Pathol Oncol Res 4, 115–120.

Guerra FS, Oliveira RG, Fraga CAM, Mermelstein CDS, Fernandes PD (2017). ROCK inhibition with Fasudil induces beta-catenin nuclear translocation and inhibits cell migration of MDA-MB 231 human breast cancer cells. Sci Rep 7, 13723.

Guo R, Liu T, Shasaltaneh MD, Wang X, Imani S, Wen Q (2022). Targeting adenylate cyclase family: new concept of targeted cancer therapy. Front Oncol 12, 829212.

Hall E, Dekker Nitert M, Volkov P, Malmgren S, Mulder H, Bacos K, Ling C (2018). The effects of high glucose exposure on global gene expression and DNA methylation in human pancreatic islets. Mol Cell Endocrinol 472, 57–67.

Hapach LA, Mosier JA, Wang W, Reinhart-King CA (2019). Engineered models to parse apart the metastatic cascade. NPJ Precis Oncol 3, 20.

Harborg S, Zachariae R, Olsen J, Johannsen M, Cronin-Fenton D, Bøggild H, Borgquist S (2021). Overweight and prognosis in triple-negative breast cancer patients: a systematic review and meta-analysis. NPJ Breast Cancer 7, 119.

Hayes JS, Brunton LL, Mayer SE (1980). Selective activation of particulate cAMP-dependent protein kinase by isoproterenol and prostaglandin E1. J Biol Chem 255, 5113–5119.

Hirayama A, Kami K, Sugimoto M, Sugawara M, Toki N, Onozuka H, Kinoshita T, Saito N, Ochiai A, Tomita M, *et al.* (2009). Quantitative metabolome profiling of colon and stomach cancer microenvironment by capillary electrophoresis time-of-flight mass spectrometry. Cancer Res 69, 4918–4925.

Kim MO, Ryu JM, Suh HN, Park SH, Oh YM, Lee SH, Han HJ (2015). cAMP promotes cell migration through cell junctional complex dynamics and actin cytoskeleton remodeling: implications in skin wound healing. Stem Cells Dev 24, 2513–2524.

Kim T-H, Vazquez-Hidalgo E, Abdou A, Tan XHM, Christodoulides A, Farris CM, Chiou P-Y, Sloan EK, Katira P, Rowat AC (2019). β-Adrenergic signaling modulates cancer cell mechanotype through a RhoA-ROCK-myosin II axis. bioRxiv, 777755, doi: https://doi.org/10.1101/777755.

Kim TH, Gill NK, Nyberg KD, Nguyen AV, Hohlbauch SV, Geisse NA, Nowell CJ, Sloan EK, Rowat AC (2016). Cancer cells become less deformable and more invasive with activation of β-adrenergic signaling. J Cell Sci 129, 4563–4575.

Kondo H, Ratcliffe CDH, Hooper S, Ellis J, MacRae JI, Hennequart M, Dunsby CW, Anderson KI, Sahai E (2021). Single-cell resolved imaging reveals intra-tumor heterogeneity in glycolysis, transitions between metabolic states, and their regulatory mechanisms. Cell Rep 34, 108750.

Kopperud R, Krakstad C, Selheim F, Døskeland SO (2003). cAMP effector mechanisms. Novel twists for an "old" signaling system. FEBS Lett 546, 121–126.

Kraning-Rush CM, Califano JP, Reinhart-King CA (2012). Cellular traction stresses increase with increasing metastatic potential. PLoS One 7, e32572.

Krzeslak A, Wojcik-Krowiranda K, Forma E, Jozwiak P, Romanowicz H, Bienkiewicz A, Brys M (2012). Expression of GLUT1 and GLUT3 glucose transporters in endometrial and breast cancers. Pathol Oncol Res 18, 721–728.

Kumar S, Weaver VM (2009). Mechanics, malignancy, and metastasis: the force journey of a tumor cell. Cancer Metastasis Rev 28, 113–127.

Laudański P, Swiatecka J, Kovalchuk O, Wołczyński S (2003). Expression of GLUT1 gene in breast cancer cell lines MCF-7 and MDA-MB-231. Ginekol Pol 74, 782–785.

Liberti MV, Locasale JW (2016). The Warburg effect: how does it benefit cancer cells? Trends Biochem Sci 41, 211–218.

Lin HH, Lee TY, Liu TW, Tseng CP (2017). High glucose enhances cAMP level and extracellular signal-regulated kinase phosphorylation in

Chinese hamster ovary cell: usage of Br-cAMP in foreign protein β-galactosidase expression. J Biosci Bioeng 124, 108–114.
Liu Z, Lee SJ, Park S, Konstantopoulos K, Glunde K, Chen Y, Barman I (2020). Cancer cells display increased migration and deformability in pace with metastatic progression. Faseb j 34, 9307–9315.
Lorenowicz MJ, Fernandez-Borja M, Hordijk PL (2007). cAMP signaling in leukocyte transendothelial migration. Arterioscler Thromb Vasc Biol 27, 1014–1022.
Lyons TG (2019). Targeted therapies for triple-negative breast cancer. Curr Treat Options Oncol 20, 82.
Macheda ML, Rogers S, Best JD (2005). Molecular and cellular regulation of glucose transporter (GLUT) proteins in cancer. J Cell Physiol 202, 654–662.
Martyn JA, Kaneki M, Yasuhara S (2008). Obesity-induced insulin resistance and hyperglycemia: etiologic factors and molecular mechanisms. Anesthesiology 109, 137–148.
Matsui C, Takatani-Nakase T, Maeda S, Nakase I, Takahashi K (2017). Potential roles of GLUT12 for glucose sensing and cellular migration in MCF-7 human breast cancer cells under high glucose conditions. Anticancer Res 37, 6715–6722.
Medina RA, Owen GI (2002). Glucose transporters: expression, regulation and cancer. Biol Res 35, 9–26.
Monzo P, Crestani M, Chong YK, Ghisleni A, Hennig K, Li Q, Kakogiannos N, Giannotta M, Richichi C, Dini T, *et al.* (2021). Adaptive mechanoproperties mediated by the formin FMN1 characterize glioblastoma fitness for invasion. Dev Cell 56, 2841–2855.e2848.
Murrell M, Oakes PW, Lenz M, Gardel ML (2015). Forcing cells into shape: the mechanics of actomyosin contractility. Nat Rev Mol Cell Biol 16, 486–498.
Nakagawa Y, Nagasawa M, Medina J, Kojima I (2015). Glucose evokes rapid Ca2+ and cyclic AMP signals by activating the cell-surface glucose-sensing receptor in pancreatic β-cells. PLoS One 10, e0144053.
Newell-Litwa KA, Horwitz R, Lamers ML (2015). Non-muscle myosin II in disease: mechanisms and therapeutic opportunities. Disease Models & Mechanisms 8, 1495–1515.
Nordlie RC, Foster JD, Lange AJ (1999). Regulation of glucose production by the liver. Annu Rev Nutr 19, 379–406.
Núñez Abad M, Calabuig-Fariñas S, Lobo de Mena M, José Godes Sanz de Bremond M, García González C, Torres Martínez S, García-García J, Iranzo González-Cruz V, Camps Herrero C (2021). Update on systemic treatment in early triple negative breast cancer. Ther Adv Med Oncol 13, 1758835920986749.
Ochalek T, Nordt FJ, Tullberg K, Burger MM (1988). Correlation between cell deformability and metastatic potential in B16-F1 melanoma cell variants. Cancer Res 48, 5124–5128.
Oishi A, Makita N, Sato J, Iiri T (2012). Regulation of RhoA signaling by the cAMP-dependent phosphorylation of RhoGDIα. J Biol Chem 287, 38705–38715.
Okeyo KO, Adachi T, Sunaga J, Hojo M (2009). Actomyosin contractility spatiotemporally regulates actin network dynamics in migrating cells. J Biomech 42, 2540–2548.
Okumura M, Yamamoto M, Sakuma H, Kojima T, Maruyama T, Jamali M, Cooper DR, Yasuda K (2002). Leptin and high glucose stimulate cell proliferation in MCF-7 human breast cancer cells: reciprocal involvement of PKC-alpha and PPAR expression. Biochim Biophys Acta 1592, 107–116.
Palorini R, Cammarata FP, Balestrieri C, Monestiroli A, Vasso M, Gelfi C, Alberghina L, Chiaradonna F (2013). Glucose starvation induces cell death in K-ras-transformed cells by interfering with the hexosamine biosynthesis pathway and activating the unfolded protein response. Cell Death Dis 4, e732.
Pinheiro C, Sousa B, Albergaria A, Paredes J, Dufloth R, Vieira D, Schmitt F, Baltazar F (2011). GLUT1 and CAIX expression profiles in breast cancer correlate with adverse prognostic factors and MCT1 overexpression. Histol Histopathol 26, 1279–1286.
Pinto C, Papa D, Hübner M, Mou TC, Lushington GH, Seifert R (2008). Activation and inhibition of adenylyl cyclase isoforms by forskolin analogs. J Pharmacol Exp Ther 325, 27–36.
Protani M, Coory M, Martin JH (2010). Effect of obesity on survival of women with breast cancer: systematic review and meta-analysis. Breast Cancer Res Treat 123, 627–635.
Pushkarsky I, Tseng P, Black D, France B, Warfe L, Koziol-White CJ, Jester WF, Jr, Trinh RK, Lin J, Scumpia PO, *et al.* (2018). Publisher correction: elastomeric sensor surfaces for high-throughput single-cell force cytometry. Nat Biomed Eng 2, 265.
Qi D, Kaur Gill N, Santiskulvong C, Sifuentes J, Dorigo O, Rao J, Taylor-Harding B, Ruprecht Wiedemeyer W, Rowat AC (2015). Screening cell mechanotype by parallel microfiltration. Sci Rep 5, 17595.
Qiu J, Zheng Q, Meng X (2021). Hyperglycemia and chemoresistance in breast cancer: from cellular mechanisms to treatment response. Front Oncol 11, 628359.
Raina H, Zacharia J, Li M, Wier WG (2009). Activation by Ca2+/calmodulin of an exogenous myosin light chain kinase in mouse arteries. J Physiol 587, 2599–2612.
Ritchie ME, Phipson B, Wu D, Hu Y, Law CW, Shi W, Smyth GK (2015). Limma powers differential expression analyses for RNA-sequencing and microarray studies. Nucleic Acids Res 43, e47.
Sarfati D, Koczwara B, Jackson C (2016). The impact of comorbidity on cancer and its treatment. CA Cancer J Clin 66, 337–350.
Sassone-Corsi P (2012). The cyclic AMP pathway. Cold Spring Harb Perspect Biol 4.
Schmidt G, Sehr P, Wilm M, Selzer J, Mann M, Aktories K (1997). Gln 63 of Rho is deamidated by *Escherichia coli* cytotoxic necrotizing factor-1. Nature 387, 725–729.
Shin E, Koo JS (2021). Glucose metabolism and glucose transporters in breast cancer. Front Cell Dev Biol 9, 728759.
Sun H, Zou J, Chen L, Zu X, Wen G, Zhong J (2017). Triple-negative breast cancer and its association with obesity. Mol Clin Oncol 7, 935–942.
Sun S, Sun Y, Rong X, Bai L (2019). High glucose promotes breast cancer proliferation and metastasis by impairing angiotensinogen expression. Biosci Rep 39.
Surdo NC, Berrera M, Koschinski A, Brescia M, Machado MR, Carr C, Wright P, Gorelik J, Morotti S, Grandi E, *et al.* (2017). FRET biosensor uncovers cAMP nano-domains at β-adrenergic targets that dictate precise tuning of cardiac contractility. Nat Commun 8, 15031.
Szablewski L (2013). Expression of glucose transporters in cancers. Biochim Biophys Acta 1835, 164–169.
Takatani-Nakase T, Matsui C, Maeda S, Kawahara S, Takahashi K (2014). High glucose level promotes migration behavior of breast cancer cells through zinc and its transporters. PLoS One 9, e90136.
The Lancet Gastroenterology, and Hepatology (2021). Obesity: another ongoing pandemic. Lancet Gastroenterol Hepatol 6, 411.
Torre D, Lachmann A, Ma'ayan A (2018). BioJupies: automated generation of interactive notebooks for RNA-Seq data analysis in the cloud. Cell Syst 7, 556–561. e553.
Welch DR, Hurst DR (2019). Defining the hallmarks of metastasis. Cancer Res 79, 3011–3027.
Wick AN, Drury DR, Nakada HI, Wolfe JB (1957). Localization of the primary metabolic block produced by 2-deoxyglucose. J Biol Chem 224, 963–969.
Wu Q, Li B, Li Z, Li J, Sun S, Sun S (2019). Cancer-associated adipocytes: key players in breast cancer progression. J Hematol Oncol 12, 95.
Wuest M, Hamann I, Bouvet V, Glubrecht D, Marshall A, Trayner B, Soueidan OM, Krys D, Wagner M, Cheeseman C, *et al.* (2018). Molecular imaging of GLUT1 and GLUT5 in breast cancer: a multitracer positron emission tomography imaging study in mice. Mol Pharmacol 93, 79–89.
Yu W, Lu QY, Sharma S, Ly C, Di Carlo D, Rowat AC, LeClaire M, Kim D, Chow C, Gimzewski JK, *et al.* (2020). Single cell mechanotype and associated molecular changes in urothelial cell transformation and progression. Front Cell Dev Biol 8, 601376.
Yu W, Sharma S, Rao E, Rowat AC, Gimzewski JK, Han D, Rao J (2022). Cancer cell mechanobiology: a new frontier for cancer research. Journal of the National Cancer Center 2, 10–17.
Zhang H, Kong Q, Wang J, Jiang Y, Hua H (2020). Complex roles of cAMP-PKA-CREB signaling in cancer. Exp Hematol Oncol 9, 32.
Zhang K, Chen L, Zheng H, Zeng Y (2022). Cytokines secreted from adipose tissues mediate tumor proliferation and metastasis in triple negative breast cancer. BMC Cancer 22, 886.
Zhang S, Ke Z, Yang C, Zhou P, Jiang H, Chen L, Li Y, Li Q (2021). High glucose causes distinct expression patterns of primary human skin cells by RNA sequencing. Front Endocrinol (Lausanne) 12, 603645.
Zhao C, Wu M, Zeng N, Xiong M, Hu W, Lv W, Yi Y, Zhang Q, Wu Y (2020). Cancer-associated adipocytes: emerging supporters in breast cancer. J Exp Clin Cancer Res 39, 156.
Zimmerman NP, Roy I, Hauser AD, Wilson JM, Williams CL, Dwinell MB (2015). Cyclic AMP regulates the migration and invasion potential of human pancreatic cancer cells. Mol Carcinog 54, 203–215.